Special Issue Papers

An Overview of the Modified Chemical Vapor Deposition (MCVD) Process and Performance

SUZANNE R. NAGEL, J. B. MACCHESNEY, AND KENNETH L. WALKER

(Invited Paper)

Abstract—**This paper reviews the MCVD process, with special emphasis on fiber design and material choices, understanding of mechanisms involved in the process, process improvements, and performance.**

I. INTRODUCTION

SINCE the initial suggestion by Kao and Hockman [1] in 1966 that low loss silica-based fibers could be used as a transmission medium in the near infrared frequency region, there has been tremendous progress in the development of processing techniques to fabricate lightguides which exhibit low attenuation, high bandwidth, good dimensional control, and excellent mechanical properties. Several processing techniques have demonstrated excellent performance as well as manufacturability: OVPO [2], MCVD [3], VAD [4], the double crucible technique [5], and PCVD [6]. This paper will review the MCVD technique, focusing on the process and mechanisms involved, as well as the resultant fiber performance and manufacturability.

The MCVD process was first reported by MacChesney *et al.* [7], [8], and has been widely used because it was relatively easy to implement. Subsequent studies have focused on understanding the fundamental physics and chemistry of the process, and establishing process controls and limits in order to realize the best geometric, optical, and mechanical performance. Upon the basis of this understanding, modification and scale-up of the process have been accomplished to improve both cost effectiveness and manufacturability. The results of this evolutionary process and its impact on fabrication will be reviewed.

II. DESCRIPTION OF THE PROCESS

The MCVD process is based on the high temperature oxidation of reagents inside a rotating tube which is heated by an external heat source. A schematic of the process, as currently practiced, is depicted in Fig. 1, while Fig. 2 shows a flow diagram of the various steps in the process.

Manuscript received September 25, 1981; revised December 1, 1981.
The authors are with Bell Laboratories, Murray Hill, NJ 07974.

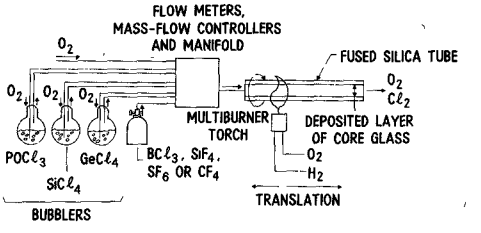

Fig. 1. Schematic diagram of MCVD apparatus.

MCVD FLOW DIAGRAM

TUBE CHARACTERIZATION
TUBE CLEANING
TUBE SET UP
HIGH TEMPERATURE FIRE POLISH - 1600-2000°C
CHEMICAL REACTION - >1300°C
NUCLEATION AND GROWTH OF PARTICLES >1300°C
PARTICLE DEPOSITION $T_{WALL} < T_{GAS}$
CONSOLIDATION 1500-1800°C
TUBE COLLAPSE 1900-2100°C
PREFORM CHARACTERIZATION
FIBER DRAWING AND COATING
PROOF TEST
FIBER CHARACTERIZATION

Fig. 2. Process steps for preparing lightguides by the MCVD technique.

Chemical reagents are first entrained in a gas stream in controlled amounts by either passing carrier gases such as O_2, Ar, or He through liquid dopant sources, or by using gaseous dopants. Halides which have reasonably high vapor pressures at room temperature are typically used and include $SiCl_4$, SiF_4, $GeCl_4$, BCl_3, BBr_3, PCl_3, $POCl_3$, SF_6, CF_4, and CCl_2F_2.

The process takes advantage of the fact that the vapor pressure of these dopants is many orders of magnitude higher than any transition metal impurities which might be present in the starting materials and cause absorption losses [9]; thus, the entrained dopants are of very high purity relative to such contaminants. Hydrogenated species, however, typically have very similar vapor pressures as the dopants and are therefore commonly purified to remove such contaminants. The

0018-9480/82/0400-0305$00.75

photochlorination technique, reported by Barns *et al.* [10], converts chemically bound hydrogen to HCl which can then be easily separated.

The high purity gas mixture is injected into a rotating tube which is mounted in a glass working lathe and heated by a traversing oxyhydrogen torch in the same direction as gas flow. The reagents react by a homogeneous gas phase reaction at high temperatures to form glassy particles which are subsequently deposited downstream of the hot zone. The heat from the moving torch fuses the material to form a transparent glassy film. Typical deposition temperatures are sufficiently high to sinter the deposited material, but not so high as to cause distortions of the substrate tube. The torch is traversed repeatedly in order to build up, layer by layer, the desired amount of material. The composition of the layers can be varied during each traversal to build up a graded index film. Typically, 30-100 layers are deposited. Fiber design and compositional requirements determine the exact deposition program. The technique can thus be used to make both step and graded single mode and multimode structures.

As MCVD is currently practiced, a thin cladding layer is first deposited. This serves as a barrier to diffusion of any impurities, such as OH, which could degrade the optical attenuation [8], [11]-[14]. In addition, the deposited cladding is a low loss material compared to the substrate tube; in both single mode and multimode fibers, a finite amount of power is propagated in the cladding, depending on the fiber design. Sufficient low loss cladding is necessary to assure low attenuation [15]. After the cladding is deposited, the core material is laid down according to a programmed chemical delivery rate. The overall efficiency of material incorporation is typically between 40-70 percent, but the incorporation of GeO_2 is quite low relative to SiO_2. The chemistry and deposition mechanisms involved will be discussed in subsequent sections.

Following deposition, the tube and deposit are collapsed to a solid rod called a preform by heating to temperatures sufficient to soften the substrate tube. The preform is then transferred to a fiber drawing apparatus where it is drawn and coated. The structure of the fiber exactly replicates the preform.

III. Material Choices and Fiber Design

Three basic fiber types of current importance are step index multimode, graded index multimode, and single mode, with the latter two of greatest interest. There has been a historical evolution of both multimode and single mode fiber design, both in terms of composition and dimensions. Design has been dictated by performance in such areas as attenuation, bandwidth, numerical aperture, bend sensitivity, splice loss, and mechanical properties, as well as the cost of the final product. The MCVD process has demonstrated tremendous flexibility in the ability to fabricate fibers of a wide variety of designs, compositions, and dimensions, and many of the fundamental studies have utilized fibers made by this process.

Silica is the primary glass former used in lightguide fabrication. Additions are made in order to alter its refractive index and build a waveguide structure. GeO_2 is the predominant dopant for increasing the refractive index of SiO_2 in MCVD [7], [8], [16]. B_2O_3 is added to decrease the viscosity and thus improve process temperatures, and decreases the refractive index [7], [8], [17]. Another additive, P_2O_5, increases the index, and has the advantage of greatly reducing the viscosity and scattering of the resultant glasses [13], [18], [19]. Fluorine can also be added to SiO_2 to reduce the index [20], [21]. The various dopants can be added in controlled amounts to make a variety of glass compositions which have refractive indexes which are less than, equal to, or higher than SiO_2, yet process at lower temperatures. Recently, considerable work has been reported on using fluorine in combination with other dopants to make a wide variety of single mode fiber designs [22]-[25].

Typical systems for the core and deposited cladding of multimode and single mode fibers made by the MCVD process are shown in Fig. 3. The choice of composition affects both the optical properties of the resultant lightguide as well as the processibility. Historically, there has been an evolution of compositions used in MCVD. Initial multimode fibers were based on GeO_2-SiO_2 cores, with a thin B_2O_3-SiO_2 barrier layer. B_2O_3 was added to the core to reduce the processing temperatures and thus avoid tube shrinkage [7], [8], [16]. Payne and Gambling first reported on doping SiO_2 with P_2O_5 [18], and fibers based on the GeO_2-P_2O_5-SiO_2 system were developed by Osanai [13] and Sommer *et al.* [19]. The substitution of P_2O_5 for B_2O_3 resulted in many beneficial effects: lower fusion temperatures, thus easier processing; lower Rayleigh scattering, thus lower loss; and yet better long wavelength loss, due to the elimination of the boron associated infrared absorption tail. Similarly, early single mode fibers were based on glasses in the SiO_2-B_2O_3 system and were quite suitable for shorter wavelength applications. With increased interest in optimizing single mode fibers for long wavelength (1.3-1.55 μm) applications, boron has been eliminated as a dopant, and a variety of structures based on core and deposited cladding glasses in the system SiO_2-GeO_2-F-P_2O_5 are being explored by various investigators [22]-[25].

The basic design of a lightguide consists of a core glass surrounded by a cladding glass of lower refractive index n. The numerical aperture NA is a function of the refractive index difference Δn between the core n_1 and cladding n_2 [26]:

$$\mathrm{NA} = (n_1^2 - n_2^2)^{1/2} \approx n_1 \sqrt{2\Delta}$$

where $\Delta = \Delta n / n_1$.

The fiber NA and core diameter $2a$ determine the number of optical modes which propagate. These are related to the normalized frequency V, given by

$$V = \frac{2\pi a}{\lambda} (\mathrm{NA}) = \frac{2\pi a n_1}{\lambda} \sqrt{2\Delta} \tag{2}$$

where λ = wavelength of light.

To achieve single mode transmission in an idealized step index fiber, V must be < 2.405 [26]. The wavelength at which the fiber becomes single mode is termed the cutoff wavelength λ_c.

Attenuation is an important consideration in fiber design.

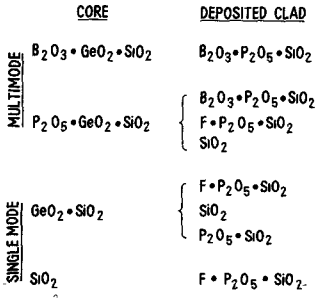

Fig. 3. Typical MCVD lightguide compositions for single mode and multimode fiber.

The intrinsic loss α_i of high silica glasses in the near infrared region of the spectrum is composed of three components [26]:

$$\alpha_i = \alpha_{UV} + \alpha_{IR} + \alpha_R \tag{3}$$

where α_{UV} = ultraviolet absorption, α_{IR} = infrared absorption, and α_R = Rayleigh scattering.

Ultraviolet absorption is determined by the electronic bandgap of a material and decays exponentially with increasing wavelength. The tail of the UV edge in glasses is almost negligibly small in the near infrared. In typical lightguide compositions, the UV absorption is due to GeO_2, as reported by Schultz [27]. The UV contribution to the loss at any wavelength can be expressed as a function of the mole fraction x of GeO_2 [28]:

$$\alpha_{UV} = \frac{154.2x}{46.6x + 60} \times 10^{-2} \exp\left(\frac{4.63}{\lambda}\right). \tag{4}$$

The infrared absorption tail results from very strong cation-oxygen vibrational modes of the glass lattice at long wavelengths. The fundamental vibrational bands of B-O, P-O, Si-O, and Ge-O occur at 7.3, 8.0, 9.2, and 11.0 μm, respectively, in high silica glass and extend to shorter wavelengths [29]. Izawa *et al.* [30] reported the absorption spectra for GeO_2-, P_2O_5-, and B_2O_3-doped fused silica over the 3-25 μm range. The extension of the B_2O_3 tail is especially deleterious to the loss, even at wavelengths as low as 1.2 μm, thereby making it an unsuitable dopant for long wavelength applications. The IR edge for GeO_2-doped silica was expressed by Miya *et al.* [28] as

$$\alpha_{IR} = 7.81 \times 10^{11} \times \exp\left(\frac{-48.48}{\lambda}\right). \tag{5}$$

This constituent makes a small contribution to the loss at 1.6 μm. Irven [31] has recently reported on the effect of P_2O_5 in the 1.6 μm region and postulated that the added loss is consistent with the P-O phonon absorption. The effect increases with increasing P_2O_5.

Rayleigh scattering results from compositional and density fluctuations over distances much smaller than the wavelength of light, and decays with the fourth power of wavelength, as expressed by

$$\alpha_R = A\lambda^{-4}$$

where A is the Rayleigh scattering coefficient, expressed in units of dB/km · μm^4. Fig. 4, after Olshansky [32], summarizes the Rayleigh scattering coefficients for a number of

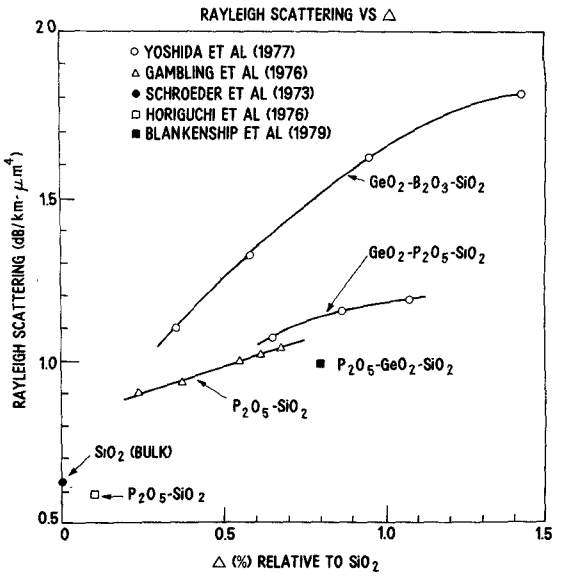

Fig. 4. Rayleigh scattering coefficient as a function of normalized refractive index difference for various lightguide compositions.

lightguide glasses reported in the literature [33]-[37] as a function of refractive index difference Δ relative to SiO_2. These data clearly show the compositional sensitivity of scattering loss. Small additions of P_2O_5 markedly reduce the Rayleigh scattering compared to B_2O_3, as Sommer *et al.* [19] and Blankenship *et al.* [37] reported that higher levels of P_2O_5 with decreased GeO_2, to achieve the same Δ, even further reduces scattering. In general, the higher the Δ of the fiber, typically accomplished by increasing GeO_2 levels, the higher the intrinsic loss levels.

An intrinsic transmission window exists between the infrared and ultraviolet losses, with the minimum loss occurring in the 1.55 μm region for fibers lightly doped with GeO_2 [28]. However, extrinsic loss mechanisms due to impurities, imperfections, and fiber design in regard to bend sensitivity can cause additional attenuation.

Transition metal ions at the level of a few ppb's can cause unacceptably high absorption losses in lightguides [1], [38]. The optical absorption of 3d transition elements in fused silica was reported by Schultz [39]. In fibers prepared by MCVD, loss due to transition metal impurities is not a problem.

Another source of absorption is due to hydroxyl ions in the glass structure. In silica-based glasses, a strong fundamental Si-OH vibration occurs at ~2.7 μm and results in a first and second overtone at 1.38 and 0.95 μm, respectively, and a combination overtone at 1.25 μm [40], [41]. For every ppm OH, losses of 48 dB/km at 1.39 μm, 2.5 dB/km at 1.25 μm, and 1.2 dB/km at 0.95 μm are added; thus, very low levels of OH are necessary to achieve low loss at long wavelengths, especially because the peaks are relatively broad. The exact peak position and width are a function of composition [32], with additions of GeO_2 moving the peak to longer wavelengths [42].

When P_2O_5 is added to SiO_2, a new and very broad band appears at 3.05 μm, attributed to the fundamental P-OH stretch [43]. The first overtone of this band is quite broad in the 1.5-1.7 μm region, and has been reported by Blankenship *et al.* [37] and Edahiro *et al.* [44]. The higher either the P_2O_5 or

OH content, the greater the added loss. Thus, fibers for use in this region of the spectrum must either have extremely low OH levels or avoid P_2O_5 as a dopant.

Other sources of loss in fibers are due to waveguide imperfections such as bubbles and defects, microbending or other bend sensitivity due to fiber design or coating irregularities, and interfacial scattering. Typically, such effects give rise to loss which is independent of wavelength.

Inada [45] proposed a graphical method to analyze fiber loss mechanisms by using the relationship that loss α is

$$\alpha = A\lambda^{-4} + B + C(\lambda) \tag{7}$$

where A is the Rayleigh scattering coefficient, B is wavelength-independent loss, and $C(\lambda)$ is any loss mechanism that has a wavelength-dependent component. By plotting α versus λ^{-4}, a straight line is obtained whose slope is A and intercept is B. Deviations from linearity are $C(\lambda)$, such as an OH peak. At shorter wavelengths (< 0.7 μm), deviations have been observed which have been attributed to a number of different effects: drawing induced coloration [46], [47], drawing induced loss [23], [48], and UV damage [49], [50]. Radiation can also affect the fiber loss, as reviewed by Friebele [51]. In single mode fibers, loss beyond λ_c can occur due to poor mode confinement [24], [25].

Dispersion in fibers determines the bandwidth performance. In multimode fibers there are two sources of dispersion: intermodal dispersion due to delay differences among the modes and chromatic dispersion resulting from the spectral width of the light source. The intermodal dispersion is controlled by the shape of the refractive index profile, and can be minimized by having a power-law shaped profile of the form [52]

$$n(r) = n_1 [1 - \Delta(r/a)^{\alpha}] \tag{8}$$

where α = profile parameter.

The value of the optimal α for any wavelength of operation is affected by the material dispersion of the lightguide [53].

Material dispersion M is due to the wavelength dependence of the refractive index and is expressed by [54]

$$M = \frac{\lambda}{c}\frac{d^2n}{d\lambda^2} \tag{9}$$

where c = speed of light.

M is a function of glass composition, and for high silica compositions, there is a zero dispersion wavelength λ_0 which corresponds to where $d^2n/d\lambda^2 = 0$ that is in the region of 1.3 μm [55]. Malitson [56] found $\lambda_0 = 1.274$ μm for fused SiO_2. Additions of GeO_2 increase λ_0 [57]-[62]; P_2O_5 is not thought to shift λ_0 [59], [61]; B_2O_3 [57], [60], [62] and F [63] doping slightly decrease λ_0.

Olshansky and Keck [53], taking into account material dispersion effects, predict an optimal α profile described by

$$\alpha = 2 - P - \frac{12\Delta}{5}. \tag{10}$$

P is defined as the optimal profile dispersion parameter

$$P = \frac{n_1}{N_1}\frac{\lambda}{\Delta}\frac{d\Delta}{d\lambda} \tag{11}$$

and N_1 is the group index $= n_1 - \lambda(dn/d\lambda)$. They assumed constant profile dispersion across the core.

The optimal α is thus a function of composition. In binary P_2O_5-SiO_2 glass there is very little variation of α_{opt} with wavelength because of the similar material dispersion characteristics [64]. GeO_2-SiO_2 compositions [32], [57] have a very strong dependence of α_{opt} on wavelength. Ternary GeO_2-P_2O_5-SiO_2 will fall somewhere between, depending on the relative doping levels [19], [32], [65]. Blankenship *et al.* [37] were able to use higher P_2O_5 levels in this system in order to decrease the sharp dependence of bandwidth on wavelength. Marcatili [66] has studied the broader case where the profile dispersion is not constant, such as when B_2O_3 is added to GeO_2-SiO_2, or for high NA fibers. Peterson *et al.* [67] have used exact solutions to Maxwell's equation to predict dispersion effects. Marcuse and Presby analyzed the effect of perturbations in typical profiles of multimode MCVD fibers [68].

The source width $\Delta\lambda$ will also affect the bandwidth. Horiguchi *et al.* [69] reported the effect of $\Delta\lambda$ on the maximum bandwidth, and found that for a given profile $\alpha = 1.95$, not only did the bandwidth decrease markedly with increased $\Delta\lambda$, but the position of the maximum shifted to longer wavelengths due to its effect on intermodal dispersion. In addition, for any λ, the further away from λ_0 one is, the lower the bandwidth for a given $\Delta\lambda$, i.e., the greater the effect of chromatic dispersion.

All of the above factors affect the attainment of the theoretical bandwidth estimated for an optimal α profile. Fiber composition profile control and spectral width will determine the actual performance of MCVD lightguides.

In single mode lightguides the total dispersion is only due to chromatic dispersion, and is a function of the material dispersion and waveguide dispersion [70], [71]. The waveguide dispersion is due to the variation in the group velocity of the fundamental mode v_g with wavelength $dv_g/d\lambda$. In turn, waveguide dispersion is a function of the core radius, Δ and λ. At short wavelengths the material dispersion is dominant, but near λ_0 the contribution of waveguide dispersion approaches that of material dispersion. At wavelengths greater than λ_0, the two are opposite in sign, and thus can be counterbalanced to shift the zero total dispersion wavelength to longer wavelengths, such as 1.55 μm where the loss is minimum [28]. Thus, by balancing these two effects, single mode fibers can be designed to have λ_0 fall over a wide wavelength range. Intense investigation of single mode fiber design to optimize the fiber performance in regard to bandwidth, loss, mode confinement, bend sensitivity, and wavelength of operation have recently been reported [22]-[25]. Theoretical loss levels have been achieved in single mode fibers [28], as well as very high bandwidths.

In addition to bandwidth and attenuation, fiber design must take into account other important parameters. For multimode fibers, the dimensions and refractive index difference determine the sensitivity to bends. Olshansky [72] has shown the microbending sensitivity α_M to be

$$\alpha_M \alpha \frac{1}{\Delta^3}\frac{a^4}{d^6} \tag{12}$$

where a = core diameter and d = outer diameter. Splice loss is predominantly affected by offset, and is proportional to $(1/a)^{1.5}$ [73]. Fiber cost is related to the volume of material which must be fabricated; thus, it is also a function of the fiber diameter. Based on such considerations, the standard

multimode fiber design has evolved to have a 50 μm core, 125 μm OD with a fiber $NA = 0.20$-0.23 [74], [75]. The optimal single mode fiber design is still under evaluation.

IV. Tubing Considerations and Setup

The MCVD process starts with a tube, typically fused silica, although Vycor can also be used. The tube ultimately becomes the outer cladding in the resultant lightguide. Early MCVD configurations used small thin-walled tubes, such as 13 mm ID × 15 mm OD. The current standard process uses a 19 mm ID × 25 mm OD tube.

The tube is first dimensionally characterized for overall size, end-to-end variations, and dimensional uniformity in regard to siding and ellipticity since all of these can affect the dimensional quality of the final product. The quality of the starting tube is important since the existence of bubbles, inclusions, or other defects can affect both the strength [76] and optical attenuation of the final product. The most commonly used substrate tube is Heralux waveguide grade TO-8.

The tube is cleaned before use with typical cleaning procedures, employing both a degreasing step as well as an acid etch. This procedure assures removal of any debris or contaminants that could lead to bubbles or impurity effects.

The setup of the tube is important for controlled MCVD processing; it is mounted in a glass working lathe which has precisely aligned chucks, and is connected to the chemical delivery system by means of a swivel device. This must stay leak-tight during all phases of the operation to avoid the ingress of wet room air. The tube is aligned so it runs true, a critical step in the subsequent high temperature processing. It is then flared and connected to a larger exit tube designed to collect unincorporated particles; a stress-free joint is essential. The larger exit tube is coupled to a scrubber designed to remove chlorine and particles.

The tube is then fire polished at very high temperatures (up to 2000°C) in order to remove surface irregularities and shrink any tubing bubbles. An oxyhydrogen torch is most commonly used as the external heat source, and the tube temperature is monitored with an optical pyrometer. The signal from this can be used to feedback to a flame control module. Under optimal conditions, tube temperature is controlled to ±2°C during each traversal pass.

V. Chemistry

Various aspects of the chemistry play a key role in determining the characteristics of the final fiber product. Very little has been reported on the chemistry involved in the MCVD process. Powers [77] and French *et al.* [78] studied the kinetics of the oxidation of various reagents such as $SiCl_4$, $GeCl_4$, $POCl_3$, $SiBr_4$, and BCl_3 in the gaseous phase at high temperatures. They concluded that under normal MCVD operating conditions the reaction will go to completion. Wood *et al.* [79] reported on a technique to study reactions by direct infrared absorption spectrophotometry of the flowing gas system in MCVD. They found that the oxidation of $SiCl_4$ resulted in oxychloride formation at intermediate temperatures (900-1100°C), but at higher temperatures converted entirely to SiO_2.

Kleinert *et al.* [80] have examined the equilibria of the oxidation of $SiCl_4$ and $GeCl_4$ at high temperatures as a function of O_2 flow. Oxidation of the individual reagents was examined, and for both cases they calculated that the equilibrium was reached at high temperatures, according to the reactions

$$SiCl_4 + O_2 \rightleftharpoons SiO_2 + 2Cl_2 \tag{13}$$

$$GeCl_4 + O_2 \rightleftharpoons GeO_2 + 2Cl_2. \tag{14}$$

For $SiCl_4$, the oxidation was complete, whereas for $GeCl_4$, the amount of GeO_2 formed, as described by equilibrium calculations, was a strong function of excess oxygen. When $GeCl_4$ is oxidized in the presence of $SiCl_4$, they calculated the conversion of $GeCl_4$ to GeO_2 to be controlled by the dependence of equilibrium on temperature and the ratio of concentrations in the gaseous phase. Experimentally, they determined only 27 percent GeO_2 conversion at 2000 K.

Wood *et al.* [81] have studied the germanium chemistry experimentally using infrared spectroscopic analysis of the effluent gases, and concluded that low GeO_2 incorporation is due to unfavorable equilibria in the reaction hot zone. They examined conditions of $GeCl_4 = 0.05$ g/min, $SiCl_4 = 0.5$ g/min, $O_2 = 1500$ cm^3/min (Fig. 5). Below 1300 K, no reaction occurs. Between 1300 and 1600 K, reaction commences for $SiCl_4$ conversion to silicon oxychlorides. Above 1800 K, all $SiCl_4$ is oxidized to SiO_2. For $GeCl_4$, it only reacts partially to form GeO_2 up to temperatures of ~1800 K as determined by the effluent $GeCl_4$. However, above 1800 K the $GeCl_4$ in the effluent increases, indicating less GeO_2 formation (Fig. 5). They explained this by considering the equilibria of the reactions [13], [14] which have equilibrium constants

$$K_1 = a_{SiO_2} P^2_{Cl_2} / P_{SiCl_4} P_{O_2} \tag{15}$$

$$K_2 = a_{GeO_2} P^2_{Cl_2} / P_{GeCl_4} P_{O_2} \tag{16}$$

where a_{SiO_2}, a_{GeO_2} = activities of species in solid reaction product (these are taken as equal to the mole fraction of the constituent in the solid) and P = partial pressure of component.

The equilibrium for $SiCl_4$ is far to the right at high temperatures ($K_1 = 6 \times 10^4$ at 1800 K); thus, all $SiCl_4$ is converted to SiO_2. However, for the $GeCl_4$ equilibrium, $K_2 = 0.36$ at 1600 K and 0.17 at 2000 K, and the equilibrium is shifted to the left by the large amounts of Cl_2 produced in the oxidation of $SiCl_4$. Thus, as temperature is raised, less GeO_2 is formed and more $GeCl_4$ is detected in the effluent (Fig. 5). The minimum in the effluent partial pressure of $GeCl_4$ at ~1800 K marks the transition from the reaction being rate limited to being equilibrium limited. MCVD is typically operated at temperatures > 1800 K or in the equilibrium-limited regime.

Wood *et al.* [81] also showed that $SiBr_4$ could be substituted for $SiCl_4$, resulting in a decrease in Cl_2 concentration in the MCVD atmosphere, thus increasing the extent of $GeCl_4$ reaction. They found that the fraction of GeO_2 incorporated was increased by greater than 3×, thus providing further experimental proof that the incorporation efficiency for GeO_2 is largely controlled by equilibrium.

Thus, equilibrium considerations are important in terms of relating the input chemical delivery program to the amount of dopant incorporated in the resultant preform. The addition of $POCl_3$ and/or fluorine dopants to the MCVD gas stream further complicates the equilibrium chemistry and is currently being evaluated [82].

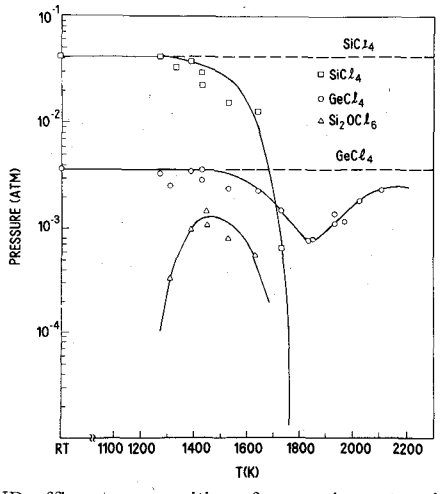

Fig. 5. MCVD effluent compositions for reactions at various temperatures, starting composition: $GeCl_4$ = 0.05 g/min; $SiCl_4$ = 0.5 g/min; O_2 = 1500 cm^3/min. Dotted line indicates initial partial pressures.

Another important aspect of MCVD chemistry is the incorporation of the impurity OH. The reduction of OH in optical fibers to very low levels has been a key to the realization of close to theoretical attenuation levels in the 1.3-1.7 μm region of the spectrum. The sources of OH contamination and the chemistry of OH incorporation must be understood and controlled in MCVD in order to achieve these very low levels, and considerable advances have been reported by many workers.

In MCVD, OH contamination has been identified as coming from three sources [13]: thermal diffusion of OH from the starting substrate tube into the core during processing; incorporation of OH from impurities in the starting reagents and carrier oxygen gas; and contamination which results from leaks in the chemical delivery system or swivel during processing. This last source of contamination can be eliminated by very careful construction and frequent leak testing of the equipment, as well as through careful processing.

Diffusion of OH into the active optical region of the fiber has been studied by a number of investigators [11]-[14] and can be eliminated by deposition of sufficiently thick low OH cladding. The remaining source of OH is that which comes in during processing either through the gas supply, reactants, or leaks in the system, and is determined by the chemistry involved in the MCVD reaction [83]. The OH level in the fiber is controlled by the reaction

$$H_2O + Cl_2 \rightleftharpoons 2HCl + \tfrac{1}{2}O_2 \tag{17}$$

which has an equilibrium constant K:

$$K = \frac{(P_{HCl})^2 (P_{O_2})^{1/2}}{(P_{H_2O})(P_{Cl_2})} \tag{18}$$

where P = partial pressure of the component.

The amount of OH incorporated into the glass C_{OH} is described by

$$C_{OH} \alpha \frac{P_{H_2O}^{initial} P_{Cl_2}^{1/2}}{P_{O_2}^{1/4}}. \tag{19}$$

During the deposition phase of MCVD, there is typically 3-10 percent Cl_2 present due to the oxidation of the chloride reactants. Wood *et al.* [84], [85] and LeSergent *et al.* [86] have shown that the chemical equilibrium results in almost all the hydrogen present being converted to HCl which is not incorporated into the glass network. The level of hydrogen contamination is reduced by a factor of ~4000. However, during collapse, chlorine is typically not present, and significant amounts of OH can be incorporated, as reported by Pearson [87].

Three approaches can therefore be taken to reduce OH contamination in MCVD: to reduce the H_2O concentration by careful processing and purification of chemicals; increasing the partial pressure of Cl_2 such as by adding it during deposition or collapse; or lowering the O_2 partial pressure such as by using an inert gas or lower excess O_2 flows.

Walker *et al.* [83] have reported that the use of a 20 percent chlorine atmosphere during collapse reduces the OH peak by >twofold for multimode fiber fabrication and >tenfold during single mode fabrication, which agrees well with the equilibrium predictions. Ainslie *et al.* [88] have also used this approach.

Fig. 6 shows the dependence of the SiOH concentration in the resultant glass as a function of the typical P_{O_2} and P_{Cl_2} conditions which occur during deposition, soot consolidation, and collapse with and without chlorine when 10 ppm H_2O is in the starting gas. The beneficial effect of chlorine during collapse is clearly demonstrated. In MCVD, practiced with Cl_2 collapse techniques, the residual water is believed to be incorporated during deposition, resulting in ~0.04 dB/km/ppm H_2O in the gas stream at 1.39 μm.

VI. Thermophoresis

Thermophoresis has been conclusively established as the particulate deposition mechanism in MCVD [89]-[92]. The basic mechanism of thermophoresis is that a suspended particle in a temperature gradient experiences a net force in the direction of decreasing temperature, resulting from the fact that molecules impacting the particle on opposite sides have different average velocities due to the temperature gradient.

Walker *et al.* [90] have reported a mathematical model for thermophoretic deposition in which they assessed the quantitative importance of thermophoresis in MCVD by considering a simple idealization of the process, and found that it predicted deposition efficiencies of the same magnitude as had been experimentally observed. A basic feature of the mathematical model was that the deposition efficiency under normal MCVD operating conditions was a function of the equilibrium temperature T_e at which the gas and tube wall equilibrate downstream of the hot zone and the temperature at which the chemical reaction to form particles T_{rxn} occurs. The deposition efficiency ϵ was given by $\epsilon \approx 0.8\ [1 - (T_e/T_{rxn})]$ where the temperature is in degrees Kelvin.

Subsequent modification of the mathematical model was made in order to compare experimentally measured efficiencies under a variety of different experimental conditions to theoretical predictions [91], [92]. This involved using measured outside wall temperature profiles, realistic effective reaction temperatures, and other relevant operating parameters to compute the temperature field within the tube and the subsequent particle trajectories which resulted from this tempera-

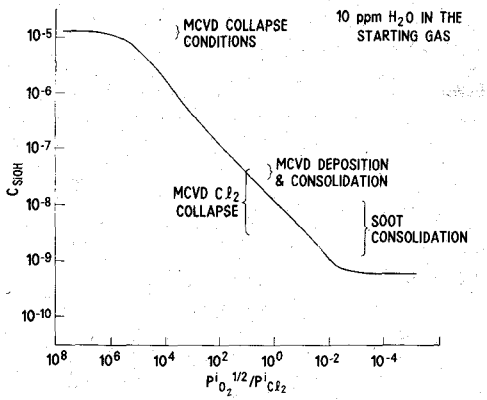

Fig. 6. Equilibrium concentration of SiOH as a function of typical partial pressures of O_2 and Cl_2 during MCVD processing for a given initial H_2O concentration (10 ppm).

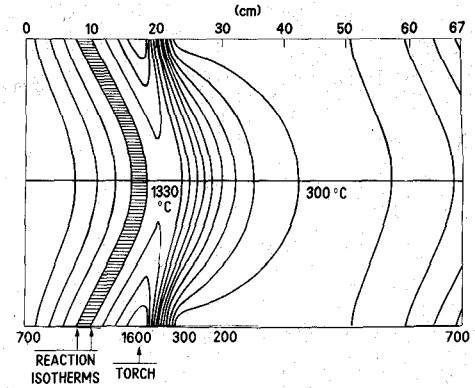

Fig. 7. Example of the temperature field inside MCVD substrate tube when heated by an external torch.

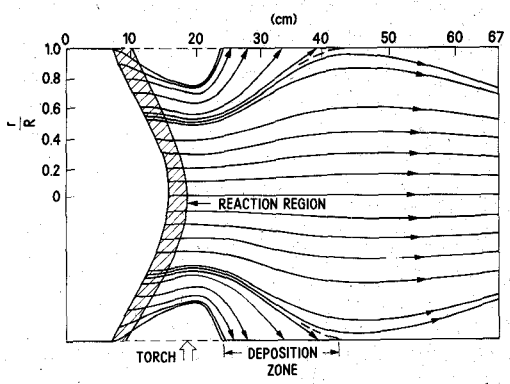

Fig. 8. Particle trajectories resulting from temperature field of Fig. 7.

ture field. They then could predict efficiencies. Fig. 7 shows one case of the temperature field within the tube, while Fig. 8 shows the resultant trajectories. As cool gas enters the hot zone it begins to heat, and at any point where the temperature $T > T_{rxn}$, a particle is formed at a particular radial position. As the gas and particle continue to flow through the hot zone, the gas heats further because the wall temperatures in the hot zone are greater than T_{rxn}, resulting in the particle moving toward the center of the tube. Further downstream the wall temperature is less than the gas temperature, resulting in the particle reversing direction and moving toward the tube wall. Certain trajectories near the wall result in particle deposition, while other particles nearer the center are swept out of the tube. Excellent agreement between the predicted and experimentally observed efficiencies for deposition of pure SiO_2 established thermophoresis as the predominant mechanism for deposition.

The model was also used to establish two distinct operating regimes in MCVD related to flow rate and thermal configuration [92]. Under normal operating conditions, the chemical reaction goes to completion within the entire tube because the temperature of the gas stream exceeds the temperature necessary for reaction [Fig. 9(a)]. In this case the process is limited by the transport of particles to the tube wall, with particles at positions $r > R_d$ depositing. Efficiency is described as $\epsilon \approx 0.8(1 - T_e/T_{rxn})$ and is most sensitive to T_e. The value of T_e will depend strongly on the torch traverse length, the torch traverse velocity, the ambient temperature, and the tube wall thickness, but is only weakly dependent on the flow rate and tube radius.

At higher flow rates, there is a region in the center of the tube where the temperature does not reach T_{rxn}, and a critical radius R_r exists such that for radial positions $r > R_r$, reaction and particle formation occur, and for positions $r < R_r$, there is no particle formation. If $R_r < R_d$, efficiency is limited by particle transport, as shown in Fig. 9(b). Fig. 9(c) illustrates the case of reaction-limited deposition where all particles formed are deposited, but particle formation is limited by incomplete reaction. Deposition is then extremely sensitive to the hot zone length, gas flow rate, gas thermal diffusivity, and especially the internal wall temperature, making controlled deposition very difficult.

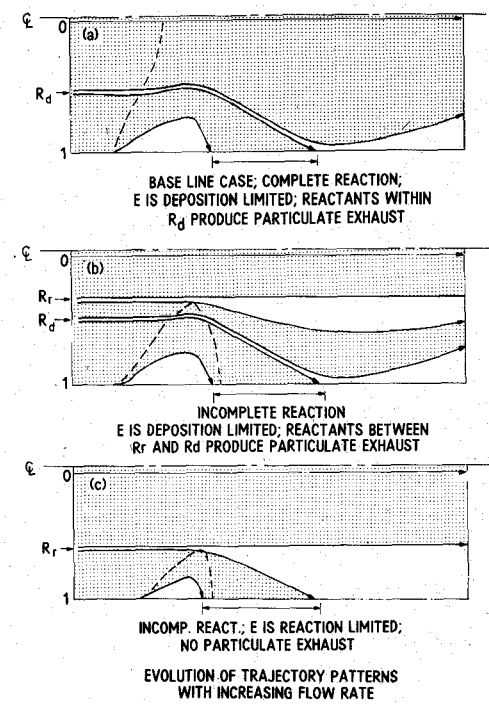

Fig. 9. Trajectory patterns as a function of increased flow.

Operation in the deposition-limited regime is preferred for maximum process control, and can be assured by using lower total flow rate Q; adding helium to the gas stream to increase the thermal diffusivity α, and using a broader hot zone, thereby more effectively heating the gases; or by operating

with higher wall temperatures. In this regime, efficiency changes only slightly with flow rate due to changes in T_e, and deposition takes place over a length L proportional to Q/α. Variations in T_e from one end of the tube to the other can result in variations in deposit thickness and thus T_e must be controlled. In addition, at the starting point of deposition there is inherent entry taper which corresponds to the value of one deposition length L. Entry taper can be minimized by low Q and/or high α.

The understanding of the thermophoretic mechanism has been a key to subsequent scale-up, high rate deposition, and optimization of the MCVD process.

VII. Consolidation

In MCVD, the consolidation mechanism has been experimentally identified as viscous sintering [93]. The rate of consolidation was shown to be inversely proportional to the modified capillary number C where

$$C = \frac{\eta l_0 (1 - \epsilon_0)^{1/3}}{\sigma t_s}$$

η = glass viscosity

l_0 = size of initial void regions

ϵ_0 = initial void fraction

σ = surface tension

t_s = characteristic sintering time ($= L_H/W$ where L_H = hot zone length, W = torch traverse velocity).

The sintering rate is therefore very sensitive to temperature, the chemical composition of the particles, primarily due to the strong dependence of glass viscosity on these variables, and on the gas thermal properties.

Walker *et al.* [93] showed that the consolidation of germanium borosilicate films proceeded both axially due to progressive heat treatment, and radially due to a composition gradient across the layer, as shown in Fig. 10. Densification is most rapid at the position closest to the tube wall where the GeO_2 content is highest and thus viscosity lowest. Kosinski *et al.* [94] have shown that consolidation of GeO_2-P_2O_5-SiO_2 films proceed by the same mechanism, but that the deposition conditions affect the compositional variation in each layer. Consolidation of pure SiO_2 films was examined, and was shown to consolidate uniformly due to the lack of composition gradient.

In all cases, consolidation results from a sintering process in which the energy required for mass transport is provided by a decrease in surface energy due to a decrease in surface area. The initial stages of consolidation proceed via the formation and growth of necks between adjoining particles where the radius of curvature is smallest, and further densification results in smooth networks of bridges which grow together slowly to form a pore-free glass layer.

The irregularly shaped closed pores present during consolidation demonstrate that diffusion of gas out of the pores is faster than the transport of glass as the pores shrink. Walker *et al.* [93] identified conditions which can lead to formation of bubbles in MCVD fabrication, either through incomplete consolidation or excessive deposition temperatures; in either case, bubbles degrade optical performance. This sensitivity to bubble growth is a function of the chemical composition of the material, the size of the closed pore (which is determined by the details of the deposition conditions), and the temperature. Therefore, proper consolidation of MCVD films requires optimization of operating conditions to avoid regimes where bubble growth can occur.

The details of the consolidation have some practical implications for proper MCVD processing as well as on optimizing and scaling up the process. Conditions which minimize the size of initial void regions as well as the void fraction will enhance the consolidation rate. It has been shown that under certain operating conditions [93] the addition of helium promotes proper consolidation. The formation of bubbles at high temperatures limits the maximum operating temperature; therefore, in order to assure complete consolidation, particularly at higher deposition rates, the sintering time must be increased such as by using a broader hot zone. Lastly, there is no fundamental limit on the thickness of a layer which can be successfully consolidated as long as the proper time-temperature relationship is realized.

VIII. Collapse

The collapse phase of MCVD has a number of practical implications, and is therefore important to understand. The collapse rate is an important component in the total preform processing time, and thus affects process economics. The collapse stability affects the dimensional performance of the final product. Finally, this high temperature phase of the process affects the resultant fiber refractive index profile by enhancement of a refractive index dip in the center of the fiber due to vaporization of volatile components such as GeO_2 and P_2O_5, and therefore can result in degradation of fiber bandwidth [95].

Both Lewis [96] and Kirchoff [97] have reported on the collapse of viscous tubes. The collapse rate is related to the viscosity of both the core and cladding material, the composite tube dimensions, the surface tension of the materials, and the pressure difference between the inside and outside of the collapsing tube. The collapse rate R is roughly proportional to

$$R \alpha \frac{P_0 - P_i + (\sigma/R_{\mathrm{ID}}) + (\sigma/R_{\mathrm{OD}})}{\eta(T, C, t)}$$

where P_i = internal pressure in tube, P_0 = outside pressure on tube due to torch, σ = surface tension of glass, $R_{\mathrm{ID,OD}}$ = inside and outside radius of tube, respectively, and η = viscosity as a function of temperature T, composition C, and time t.

Extensive modeling of the details of collapse of MCVD composite tubes has recently been accomplished by Geyling and Walker [98]. Some basic conclusions on collapse rate can be drawn. The surface tension of glass is only a weak function of temperature, and therefore cannot be varied in order to enhance the collapse rate. As the tube dimensions become smaller, the surface tension term will become a larger component in determining the collapse rate at a given ΔP. The viscosity of the tube and deposit is determined not only by the composition, but also by the details of the hot zone geometry during collapse. Because viscosity decreases with increased

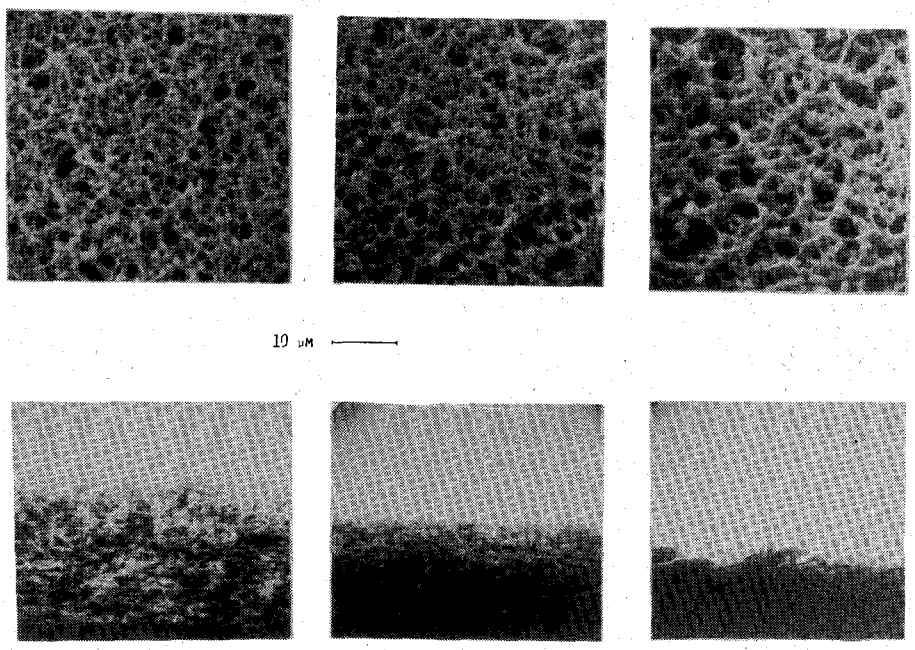

Fig. 10. SEM micrographs of the consolidation of a particulate layer in the MCVD process showing both surface (top) and cross-sectional views (bottom).

temperature, very high collapse temperatures favor fast collapse rates, but practical limitations are imposed due to fluid flow of the heated rotating tube, as well as chemical composition considerations such as those imposed by GeO volatization at the internal surface of the collapsing preform. Broader hot zones can be employed to increase collapse rate by virtue of the time-temperature effect of viscosity on the collapse rate, but again, practical limitations are imposed by heating an extended region of the tube into a regime where fluid flow can cause distortions in the collapse geometry. Nagel *et al.* [99] have reported on the optimization of collapse conditions to considerably reduce the collapse time in standard MCVD multimode preform fabrication.

Decreases in the collapse rate are only significant if coupled with the fabrication of preforms of good dimensional circularity. Geyling and Walker [98] have also modeled collapse stability. A key result in their study was the dependence of collapse stability on the initial tube geometry (wall thickness variations and ellipticity) and on the pressure difference between the inside and outside of the tube. Fig. 11 shows the dependence of the final core and cladding ellipticity on ΔP during collapse. The outside pressure is a torch stagnation pressure which results from the flow of gases as high velocities during collapse and is a function of torch design and flow rate. The inside pressure is determined by the details of the collapse procedure used. If collapse is performed with the tube open to atmosphere, tube geometry and flow rate will determine the pressure. In the case of pressurized collapse, the tube is sealed off at one end (corresponding to the right-hand end in Fig. 1) and is accomplished by heating while traversing in the opposite direction of deposition. The inside pressure can be regulated by means of a pressure-metering device. Pressure control was first effectively used by French and Tasker [100] to fabricate fibers of excellent circularity.

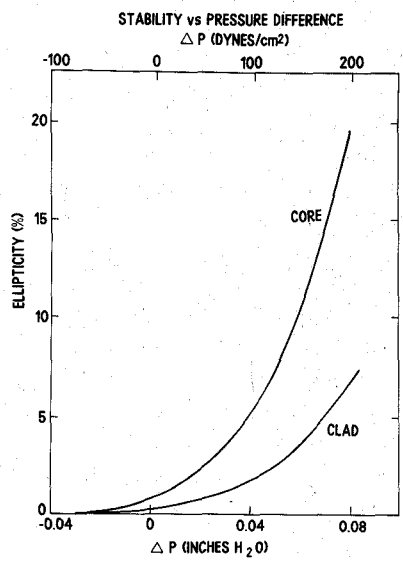

Fig. 11. Preform core and cladding ellipticity as a function of pressure difference during collapse.

The work of Geyling and Walker [98] demonstrates that in order to realize a stable geometric collapse, tube quality and pressure difference must be considered.

During the collapse phase of MCVD, very high temperatures enhance the reaction

$$GeO_2 \rightarrow GeO(\uparrow) + \tfrac{1}{2} O_2 . \tag{22}$$

Similarly, both P_2O_5 and SiO_2 can undergo volatization processes. The net effect is to cause a change in the composition of the deposited materials. Two schemes have been proposed to compensate for these effects. The first, proposed by Akamatsu *et al.* [101], uses a flowing controlled amount of $GeCl_4$ during collapse to compensate for the burnoff of GeO_2.

This technique can be used quite successfully; however, its control during collapse is difficult and is markedly affected by the specific details of any given collapse procedure, particularly when Cl_2 or $SOCl_2$ are employed as drying agents. As a result, the practical implementation of this technique is determined by empirical conditions defined by the particular preform fabricator. Another technique involves etching, which has been described by Hopland [102], and offers another alternative in processing. It also depends on an experimental definition of specific conditions in order to minimize the effect of the refractive index dip.

Optimization of the collapse phase in MCVD thus involves use of good geometric quality tubes, proper control of the length and temperature of the hot zone for a given tube geometry and relative clad/core composition and geometry, control of the pressure difference, and control of the chemistry at the inner surface of the collapsing tube.

IX. Fiber Drawing

Significant advances have been made in fiber drawing technology over the past few years, independent of the processing technique used to prepare the fiber precursor. The fiber drawing step determines the overall diameter, its variation, and to an extent, the fiber strength; it can also affect transmission properties.

Fig. 12 shows a typical state-of-the-art fiber drawing apparatus, capable of producing strong low-loss fibers with protective coatings and excellent diameter control. Blyler and DiMarcello have recently reviewed the important factors involved in the fiber draw process [103].

DiMarcello *et al.* [104] reported on the drawing of long-length high-strength fiber. His results show that as the fiber proof test level increases, the longest continuous length which can be drawn decreases. Important furnace operating parameters relating to convective flow through the furnace were defined, thus indicating the potential for achieving high yields for long-length high-strength prooftesting.

An important advance reported recently by Smithgall and Frazee [105] involved use of an automatic detection and centering technique for fibers within the applied protective coating. This technique allows fiber coating concentricity to be tightly controlled without disturbing the coating process, thus assuring no deleterious effects on the strength of the fiber or on coating-induced effects on the loss or bandwidth.

A key factor to the economic drawing and coating is fiber draw speed. Paek and Schroeder [106] have reported the capability of drawing fibers at speeds >5 m/s compared to the current standard 0.5–1.0 m/s. This required a tall draw tower to control the fiber temperature entering the coating cup and avoid menicus collapse, a special applicator to minimize shear as well as draw tension, and a high-power UV-curing system to assure proper photopolymerization.

Further work continues in the areas of long-length high-strength fiber, fiber draw speed increases, and development of coatings which result in good bend sensitivity protection and to protect the fiber from strength degradation.

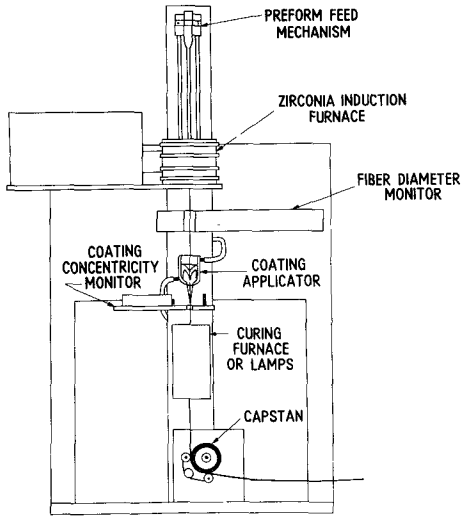

Fig. 12. Schematic of state-of-the-art fiber drawing apparatus.

X. Processing Control

The implementation of MCVD into manufacture requires material and process controls in both the preform fabrication and fiber draw stages of the process.

For maximum control of preform processing, Runk [107] reported that the following parameters should be monitored and controlled.

Geometric:

1) the geometry of the support tube, including its diameters, ovality, siding, and bow,
2) the mechanics of the setup procedures,
3) the mechanics for eliminating the initial stress and/or bow in the support tube,
4) longitudinal and radial differential thermal expansion effects,
5) process temperature variations, and
6) heat source alignment.

Optical:

1) precursor purity,
2) dopant (type and quantity),
3) dopant profile,
4) deposition rate,
5) support tube/deposition interface, and
6) preform station hardware.

Mechanical:

1) support tube quality,
2) support tube and preform handling, and
3) preform station environment.

In order to control tube geometry during deposition of highly viscous compositions which require high processing temperatures and lead to tube distortions, several workers [108], [109] have reported the use of pressurizing devices to prevent premature collapse of the tube. Most of the lightguide performance parameters (such as attenuation, numerical aperture, bandwidth, relative core/clad dimensions, and fiber and core ellipticity) will be determined during this phase of the operation.

The fiber drawing phase of the operation plays a major role in determining the fiber diameter and its control as well as strength. Runk [107] reported that the following components are critical in the fiber drawing manufacturing environment:

1) the basic structure and precision drawing mechanics,
2) a high temperature, clean heat source with appropriate temperature control,
3) diagnostic devices including precise, high rate diameter measurement,
4) a diameter feedback control system, and
5) an appropriate coating apparatus.

Very high strength fiber has been drawn using the zirconia induction furnace [76], [110], a controlled atmosphere [76], [103], careful preform handling [76], particulate free coating material [76], and a noncontacting coating applicator [111]. Excellent diameter control is achieved by using a diameter feedback control system [112], and isolating the draw process from disturbances [113].

XI. MCVD Scale-Up

The fabrication rate of preforms is an important factor affecting fiber cost. Early MCVD processes operated at deposition rates of 0.05-0.1 g/min which was much higher than conventional CVD schemes for making fiber [114], [115]. Since that time, attention has been focused on understanding the fundamental mechanisms involved in MCVD in order to scale up the process without a degradation in the optical and dimensional quality of the resultant fiber. In addition to increasing the deposition rate, accompanying decreases in the collapse time are necessary to fully optimize the process rate.

Initially the emphasis was to use MCVD to make low-loss high-bandwidth fibers, and typically low deposition rates (<0.25 g/min) were used. In fact, it was believed that higher rates degraded these properties; Osanai [13] reported that fiber loss increased with deposited layer thickness greater than ~10 μm. Akamatsu *et al.* [116] and O'Connor *et al.* [117] reported improved deposition rates by adding helium to the gas stream which enabled them to deposit and fuse thicker layers. Yoshida *et al.* [118] reported higher deposition rates (0.37 g/min) without the use of helium, accomplished by higher traverse speeds in order to minimize the layer thickness.

Nagel *et al.* [91] reported high deposition rates without a loss penalty by use of a broad hot zone which allowed layers to fuse properly. Subsequent work by Nagel and Saifi [119] reported very low losses (0.5 dB/km at 1.3 μm) over the 0.7-1.7 μm wavelength region at deposition rates up to 0.34 g/min and layer thickness of 16 μm/pass.

The understanding of the thermophoretic deposition mechanism and viscous sintering fusion mechanism has allowed the process to be further scaled up without a loss in reaction incorporation efficiency or improper fusion.

Nagel *et al.* [99] recently reported on a reduced cycle MCVD process, optimized for fabrication of preforms from a 19 mm X 25 mm tube. By adjusting the flow rate, hot zone length, and temperature to provide complete reaction, proper sintering, minimum entry taper, and avoidance of particle agglomeration, deposition rates of 0.5 g/min were achieved. They also implemented a faster collapse procedure by careful tube alignment, adjustment of the hot zone length and uniformity, proper balance of the internal pressure relative to the torch pressure, and control of the tube viscosity. Preforms capable of yielding 15 km were made in less than 7 h, and exhibited very low loss and OH (0.5 dB/km at 1.3 μm, 0.5 dB/km OH peak height at 1.39 μm), bandwidth as high as 1.8 GHz · km, and good dimensional control.

Simpson *et al.* [120], [121] and Tsukamoto *et al.* [122] have fabricated fibers at very high deposition rates (up to 1.3 g/min) by modification of the standard process. Simpson *et al.* used very high flow rates, a thinner walled silica support tube, and a very broad hot zone (accomplished by use of two torches). This was coupled with the use of water cooling of the support tube downstream of the hot zone to increase the deposition efficiency, thereby minimizing T_e and shortening the deposition length over which particle deposited. They found that the length of the water-cooled region effectively determined the deposition length L, and hence the entry taper as well. They were able to further reduce entry taper by use of helium to increase the thermal diffusivity of the gas stream. Fig. 13 shows the preform taper as a function of the various experimental conditions. Water cooling and helium resulted in small entry taper, highest rates, and uniform end-to-end dimensions. Using this technique, they have achieved losses as low as 2.8 dB/km at 0.82 and 0.7 dB/km at 1.3 μm and deposition rates on the order of 1 g/min. Tsukamoto *et al.* [122] have reported use of similar modifications to achieve deposition rates up to 1.3 g/min. They used an overcladding technique to obtain the proper clad/core diameter and were able to draw 40 km of 50 μm core 125 μm OD fiber.

Pearson [123] reported fabrication of single mode fiber at deposition rates of 0.5 g/min in a 19 mm ID X 25 mm OD tube. Losses of 0.52 dB/km at 1.3 μm and 0.28 dB/km at 1.55 μm were achieved. By using an overcladding technique, he also was able to produce a preform capable of yielding 40 km of fiber.

The evolution of increased deposition rates is shown by Fig. 14, after Cohen [124]. These have resulted in substantial increases in fiber fabrication rate, which is defined as the length of fiber produced for each hour of preform processing time, including setup, deposition, collapse, and removal. Estimates for the increase in fabrication rate if overcladding techniques [116] were used are also shown. The plasma-enhanced MCVD technique [125], to be discussed in the next section, has resulted in considerable increases in fabrication rate. Further work is being directed at optimizing high deposition rate fabrication as well as optimizing and reducing the time for collapse of scaled-up preforms, consistent with the attainment of loss, bandwidth, and dimensional performance.

XII. Plasma-Enhanced MCVD

A number of investigators have used plasma-activated processes to initiate chemical reactions within a tube in order to prepare lightguides. Both microwave plasmas (PCVD) [6], [126], [127] and RF plasmas have been studied. In PCVD, it

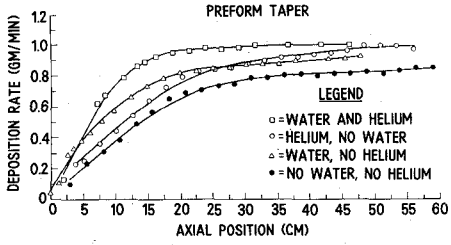

Fig. 13. Comparison of taper and core uniformity in high rate MCVD preforms prepared under different operating conditions.

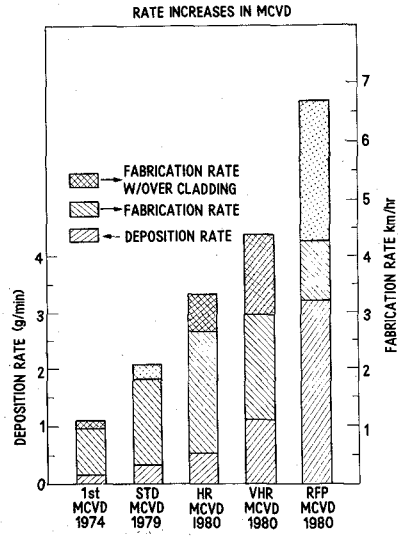

Fig. 14. Comparison of deposition rates and preform fabrication rate for laboratory MCVD processes: Early [7], standard [119], high rate [99], very high rate [122], and RF plasma MCVD [125].

is difficult to achieve deposition rates over 1.0 g/min because of the low pressures and nature of the process. RF plasma processes which operate at or near atmospheric pressure achieve high reaction rates and efficiencies. However, when the plasma is used to both initiate the chemical reaction and to sinter the deposited material, plasma instabilities are thought to have limited process performance [128]-[130].

The current plasma-enhanced MCVD technique [125], [131]-[134], a variation on conventional MCVD, embodies many improvements which have led to the fabrication of high-performance fibers at deposition rates >3.5 g/min.

Fig. 15 shows a schematic of plasma-enhanced MCVD. The technique uses an oxygen RF plasma which is operated at atmospheric pressure, and is centered in the substrate tube with an annulus of >1 cm between the visible edge of the fireball and the tube. In the initial plasma-enhanced MCVD work, the tube was traversed relative to a stationary RF coil and sintering torch, which limited the attainable traverse rate [131]. Subsequent modification by Fleming [132] used a stationary tube and simultaneously traversed the coil and torch at identical rates. This increased the attainable traverse rate as well as the length of usable preform. Further modification was recently reported by Fleming and Raju [133] in which they independently traversed the plasma and heat source which allowed independent optimization of the deposition and consolidation step.

Typical plasma operation involves use of a tube with an ID >40 mm, such as 40 mm ID $\times$ 44 or 46 mm OD tubes. Deposition rates up to 5 g/min have been reported [133]. The fused layers deposited are typically 45 to 79 μm thick and

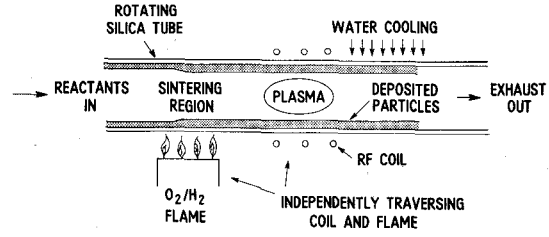

Fig. 15. Schematic of the plasma-enhanced MCVD process.

have initial densities ~65 percent theoretical. All conventional MCVD dopants can be used.

Fleming and O'Connor [131] have discussed the importance of centering the fireball, as well as the experimental conditions which affect its stability. The RF power is supplied to the coil at 3-5 MHz, resulting in typical power into the plasma of ~12 kW. The plasma fireball operates at $\sim 10^4$ °C; the high temperature of the plasma results in a large temperature gradient, thus providing a large thermophoretic driving force for efficient deposition. Flowing water continuously cools the surface of the substrate tube in the region of the plasma, thus preventing hot spots which can lead to tube distortion. This cooling also enhances plasma centering, and it minimizes T_e to further enhance efficiency. A secondary heat source is used to consolidate the deposited layers.

A key feature of the technique is the separation of the deposition and sintering steps. It has allowed stable operation of the plasma throughout deposition, and realization of very high deposition rates and efficiencies without substrate tube distortion.

Tremendous progress has been made in the preparation of high-quality high-rate preforms. Recent work has incorporated OH removal techniques to realize excellent long wavelength performance. Fig. 16 shows the best reported loss spectra for multimode [133] and single mode [134] lightguides prepared at deposition rates of 3.5 g/min. These losses are comparable to the best obtained by standard MCVD, thus providing further documentation that there is no attenuation penalty when high rate processes are optimized.

Fleming and Raju [133] also reported the effect of tube quality on optical attenuation results. Availability of tubes of proper dimensions which have the equivalent performance of tubes used in standard MCVD is the key to implementation of this technique.

Future studies are aimed at further optimization of the process. The very high deposition rates make the technique particularly suitable for single mode lightguide preparation where large amounts of deposited cladding are necessary in order to realize optimal properties.

XIII. MCVD Performance

The MCVD process has been used since its first announcement [7] to make very high performance fiber. Steady improvement has been made in the important areas of optical attenuation, fiber bandwidth, fiber strength, control of fiber bandwidth, fiber strength, control of fiber drawing and coating, and in the increasingly important area of single mode fiber preparation. Fabrication of the latter for long distance, high bit rate systems where loss, bandwidth, and bend sensitivity are critical, requires careful optimization and control of the process.

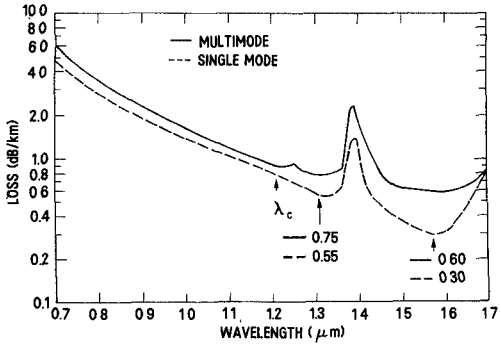

Fig. 16. Loss spectra for single mode and multimode fiber prepared by the plasma-enhanced MCVD process at 3.5 g/min.

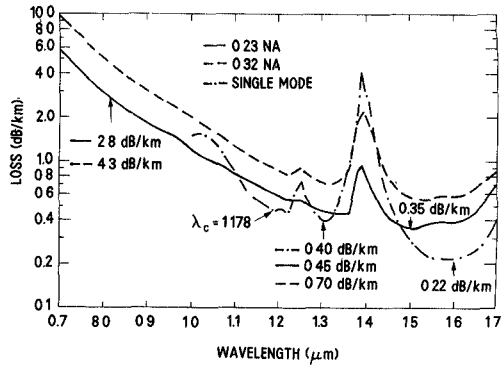

Fig. 17. Loss spectra for laboratory multimode and single mode fiber.

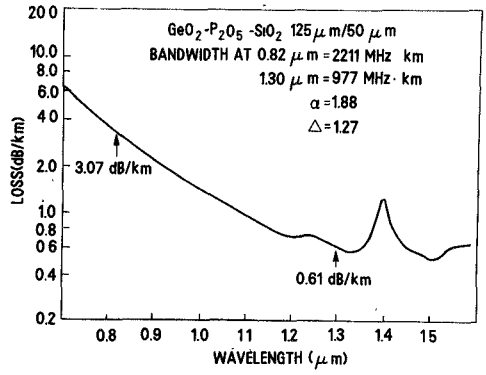

Fig. 18. Loss and bandwidth data for multimode fiber optimized for operation at two wavelengths.

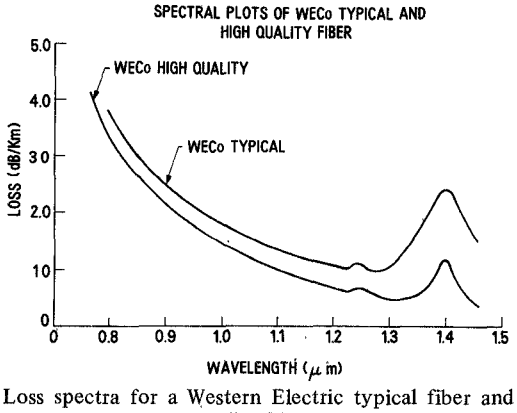

Fig. 19. Loss spectra for a Western Electric typical fiber and a high-quality fiber.

Fig. 17 shows state-of-the-art loss curves for MCVD as practiced at deposition rates of 0.5 g/min. Multimode 0.23 NA graded index germanium phosphosilicate fibers [135] show fiber losses near the intrinsic level for this composition: 2.8 dB/km at 0.82 μm, 0.45 dB/km at 1.3 μm, 0.35 dB/km at 1.5 μm, and OH peak height of 0.5 dB/km (≡10 ppb OH). Fibers of this type exhibit bandwidths >1 GHz · km and have been reported to have bandwidth as high as 1.8 GHz · km [99]. MCVD can also be used to make high-rate high-NA fiber with losses as low as 0.7 dB/km at 1.3 μm [135]. Single mode fibers prepared at high a deposition rate also show excellent loss performance, reported by Pearson [123] and Lazay *et al.* [24], as well as very low dispersion.

MCVD has been demonstrated to be capable of producing very high bandwidth. Lin *et al.* [136] reported measuring bandwidths for two different multimode 0.23 NA MCVD fibers which had maximum measured values of 4.3 GHz · km at 1.25 μm and 4.7 GHz · km at 1.29 μm, thus demonstrating that very high bandwidths, although still well below the theoretical value, can be achieved.

Fig. 18 shows fiber prepared by Partus [137], optimized for two wavelengths, which exhibits excellent loss at both 0.82 and 1.30 μm, as well as high bandwidth at both wavelengths. It was not necessary to use the approach of Blankenship *et al.* [32], [37] in which a very high phosphorous level was used to achieve this result; thus, very low loss levels in the long wavelength region were maintained.

Due to the excellent performance of MCVD fiber, a commitment to large-scale manufacture using MCVD has been made by Western Electric. Pilot plant production at Atlanta's Product Engineering Control Center (PECC) has culminated in the design and implementation of MCVD into production. Fibers produced on a 5-day, 3-shift, 24-h operation by hourly employees on multimachine assignment show excellent performance. Large-scale production of 0.23 NA, 125 μm OD, 50 μm core graded index fiber for use at two wavelengths, representing 30 000 km of fiber show median values of loss at 0.825 μm = 3.41 dB/km and at 1.3 = 1.20 dB/km; bandwidth at 0.825 μm = 825 MHz · km and at 1.3 μm = 735 MHz · km; and median OH peak height = 2.86 dB/km [138].

Fig. 19 shows the loss spectra for the typical and high-quality Western Electric product. This type of performance is comparable to the best laboratory results. Additional manufacturing experience expected to further improve loss and bandwidth of production fiber.

Manufacturing performance of single mode fiber cannot be assessed at this time. Studies on fiber design and fundamental propagation phenomena are being actively pursued by a large number of investigators. To date, MCVD has been successfully used to fabricate very high quality single mode fibers in the laboratory, and it is anticipated that further improvements will occur.

XIV. Process Comparisons

Three major fiber fabrication techniques, outside vapor phase oxidation (OVPO) [2], [139], [140], modified chemical vapor deposition (MCVD), and vapor-phase axial deposition (VAD) [4], [141]-[144], have emerged as viable processes for economic production of a high-quality multimode and single mode fiber suitable for long transmission distances at both short (0.8-0.9 μm) and long (1.3-1.6 μm) wavelengths. Direct melt fibers [5] have also demonstrated excellent short wavelength performance, but are not suitable for long wavelength operation due to water and boron absorptions, and

TABLE I
PROCESS FEATURES

	(2,139,140) OVPO	MCVD	(4,141-144) VAD
COMMON DOPANTS	SiO_2, GeO_2 P_2O_5, B_2O_3	SiO_2, GeO_2 P_2O_5, B_2O_3, F	SiO_2, GeO_2 P_2O_5, B_2O_3
REACTION MECHANISM	Flame hydrolysis of halides	Oxidation of halides	Flame hydrolysis of halides
DEPOSITION PRINCIPLE	External lateral deposition of oxide particles on rotating mandrel	Internal deposition of oxide particles on inside tube wall	End on deposition of oxide particles on rotating bait rod
DEPOSITION FEATURES	First core, then cladding deposited; Tube overcladding can be used for additional cladding	Cladding, then core deposited; tube inherent to process & provides cladding mat'l; can overclad with another tube	Core and cladding can be deposited simultaneously; tube can be used to overclad
PROCESS STEPS	Multistep process involving deposition of soot, removal of mandrel, consolidation & dehydration to form blank with or without hole, fiber drawing	Multistep process involving simultaneous deposition & consolidation, collapse to form a preform, fiber drawing	Multistep process involving deposition consolidation & dehydration to form blank, elongation, overcladding, and fiber drawing. Can potentially do all steps simultaneously & continuously.
OH CONTROL	Achieved by dehydration in controlled Cl_2 atmosphere	Achieved through leak tight system, controlled chemical purity, Cl_2 collapse technique	Achieved by dehydration in controlled Cl_2 atmosphere
PROFILE & REFRACTIVE INDEX CONTROL	Achieved by controlling and varying chemical composition of each individual deposited layer; typically 200 core layers	Achieved by controlling and varying chemical composition of each individual deposited layer; typically 50 core layers	Achieved in radial plane by control of many process variables such as torch design and positioning; H_2/O_2 ratio substrate temperature, etc.

therefore will not be considered here. The three techniques are all based on vapor phase reactions to form high silica glass structures. This section will compare some key features of these processes and review their relative performance.

Table I itemizes aspects of the processes which distinguish the three techniques, while Table II summarizes performance parameters which have been reported.

All three techniques use GeO_2 and P_2O_5 dopants to increase the refractive index relative to SiO_2 and B_2O_3 to decrease the index. However, fluorine doping, which also decreases the index without deleterious absorption at long wavelengths associated with B_2O_3, has become increasingly important, particularly in single mode structures where it permits greater fiber design flexibility. The flame hydrolysis reaction in OVPO and VAD, favoring formation of HF, is thought to prevent fluorine incorporation.

Flame hydrolysis also results in high OH levels in the deposited material in OVPO and VAD. However, because the deposited material is consolidated either as a second step or in a separate zone from deposition, the sintering conditions can be optimized for dehydration by control of the sintering atmosphere. Low partial pressures of O_2, and a Cl_2 atmosphere during consolidation minimize the OH in the resultant fiber. Thus, the hydrogen contamination levels in the starting materials is not important in OVPO and VAD. In contrast, MCVD deposition and consolidation occur simultaneously and in the same atmosphere; therefore, the amount of OH incorporated is related to the hydrogen impurity levels present during deposition and collaspe, as well as the chlorine-oxygen ratio during

TABLE II
PERFORMANCE PARAMETERS

	(2,139,140) OVPO	MCVD STD	MCVD PLASMA	(4,141-144) VAD
NA				
Typical	0.2	0.23	0.23	0.2
Max. Reported	0.3	0.38	NA	0.32
DEP. RATE (g/min.)				
Typical	1.5-2	0.35-0.5	3.5	0.3-0.5
Max. Reported	4	1.3	5.0	2
EFFICIENCY (%)	50	50	80	60
MAX. BLANK Length Reported (km)	40	40	>20	100
BEST MULTIMODE RESULTS FOR FIBER NA	0.21	0.23	0.2	0.21
Loss (dB/km)				
0.82μm	2.5	2.6	2.8	2.5
1.3	0.7	0.45	0.7	0.42
1.5-1.6μm	0.8	0.35	0.5	0.31
Bandwidth (GHz·Km)	>3	5	NA	6.5
Min.OH(ppb)	10	3	10	1

these phases of processing. Low hydrogen impurity levels in the starting materials are required for low OH levels. In OVPO, if a central hole is present during fiber drawing, control of the atmosphere to prevent OH contamination is also important. All the techniques have achieved low OH, the lowest reported in VAD (Table II).

Profile control is the key for good bandwidth performance in the resultant fiber. In both OVPO and MCVD, the resultant fiber NA and refractive index profile shape is achieved by varying the chemical delivery dopant ratios on each successive deposition pass. Relative deposition efficiency of the dopants must be taken into account to achieve the desired refractive index and profile. Profile changes can be easily made by changing the chemical delivery program. A central refractive index dip can be present in each process, as well as a ring structure corresponding to individual deposited layers. In VAD, the refractive index profile is achieved in the radial deposition plane primarily due to the spatial distribution of dopants in the flame. The torch design and position, oxyhydrogen ratio of the flame, flame temperature, dopant ratio injected through each torch nozzle, temperature distribution on the deposition surface, pressure in the deposition vessel, rotation speed and position of the porous preform end, and other process variables determine the resultant composition profile in the deposited material. A refractive index dip in the center is not present. Profile changes are achieved by a complex interaction of all the process variables; furthermore, in both OVPO and VAD the resultant concentration profile can also be altered due to dopant sublimation during the consolidation phase of the process, and thus must be accounted for in achieving the desired profile.

Each technique has produced high bandwidth fiber (Table II); however, sufficient data to make a relative bandwidth reproducibility comparison are not available.

Attenuation characteristics achieved by all three techniques are excellent (Table II). As currently practiced, processing conditions which prevent transition metal impurity contamination as well as scattering losses due to imperfections are not limiting. Further improvements in process rate, however, must be made without attenuation penalties, as well as with good bandwidth and dimensional control.

Assuming similar process yields, the relative process economics will be greatly influenced by the process rate and its complexity. All three processes, as currently practiced, consist of two major steps: preform or blank preparation and fiber drawing from the blank. The rate of fiber drawing for all processes can be the same, although in OVPO when the blank contains a central hole, the draw process must be optimized for its elimination.

In standard MCVD, preform preparation time is determined by both the deposition and collapse rates. Core deposition rates of 0.35-0.5 g/min are typical. The cladding, which in multimode fiber comprises 84 percent of the fiber volume, is predominantly provided by the substrate tube. For single mode fiber preparation, although a large amount of low-loss deposited cladding is required, the bulk of the cladding is also provided by the original support tube. Higher deposition rates, fast collapse schemes, and overcladding with a second substrate tube can further improve the process rate. In the RF-plasma-enhanced MCVD configuration, deposition rates of 3.5 g/min are typical, and the collapse phase of the process represents a larger portion of the preform preparation time. Overcladding can be used to provide additional cladding at these high deposition rates.

In contrast, in OVPO as it is currently practiced for multimode fiber preparation, both core and cladding materials are deposited, typically at 2.0 g/min. After deposition, the mandrel must be removed from the blank which is then consolidated and dehydrated in a controlled atmosphere at an optimum rate for obtaining a bubble-free, low OH glass with or, more recently, without a hole, depending on the process details. Improved process rates are possible by use of higher deposition rates, overcladding, or by simultaneously sintering and drawing fiber in the fiber drawing furnace. Information on single mode fabrication by this technique is not available.

In VAD, the core and cladding material can, in principle, be deposited simultaneously by use of multiple torches. For multimode fiber preparation, deposition of the core material as well as some cladding is typically done at 0.3-0.5 g/min/torch. The resultant soot blank can be simultaneously consolidated and dehydrated in another zone as the growing blank is undrawn through a sintering heat source, allowing for continuous blank making. Alternatively it may be consolidated off line. Typically, the sintered blank is then elongated, overclad with a silica tube, then drawn into fiber. Preparation of single mode fiber preforms, where a large amount of deposited cladding is necessary, is accomplished by use of multiple torches.

In order to compare process economics, simple comparison of deposition rates is not sufficient. For instance, if a prefabricated tube provides additional cladding, the total volume of deposited material required to produce a given volume of fiber is reduced. If a number of process steps are performed simultaneously then the process rate will be determined by the rate limiting step. The number of process steps and their complexity affect equipment requirements, labor cost, and product yield.

All three processes are potentially capable of producing high quality fiber at reasonable yield. The process rates are being constantly improved, although these improvements and the process yield are, in general, proprietary. Further improvements in these processes are anticipated. The predominance of one or more of these fabrication techniques will therefore depend on the ability to implement process rate improvements while maintaining a high yield in production.

XV. Conclusion

Since the announcement of MCVD in 1974, steady progress has been made in fiber performance and process improvements that have resulted in the large-scale manufacture of fiber by this technique. Many systems have been installed by Western Electric and other companies throughout the world using fibers made by this process, and system performance has been excellent. Further improvements in the practice of this technique are expected to result in even better performance and economy.

Acknowledgment

The authors would like to thank their many colleagues at Bell Laboratories, Western Electric Engineering Research Center, and WE-PECC for their input and contributions to this work. They are especially indebted to Western Electric per-

sonnel for their willingness to quote their data, as well as for their ongoing cooperation.

REFERENCES

[1] K. C. Kao and G. A. Hockman, "Dielectric-fiber surface waveguides for optical frequencies," *Proc. IEE*, vol. 113, no. 7, p. 1151, 1966.

[2] D. B. Keck, P. C. Schultz, and F. Zimar, U.S. Patent 3 373 292.

[3] J. B. MacChesney and P. B. O'Connor, U.S. Patent 4 217 027.

[4] T. Izawa, S. Kobayashi, S. Sudo, and F. Hanawa, in *Tech. Dig. 2nd Int. Conf. Int. Opt., Opt. Fiber Commun.*, Tokyo, Japan, 1977.

[5] G. R. Newns, K. J. Beales, and C. R. Day, in *Dig. 2nd Int. Conf., Int. Opt., Opt. Fiber Commun.*, Tokyo, Japan, 1977.

[6] J. Koenings, D. Küppers, H. Lydtin, and H. Wilson, in *Proc. 5th Conf. Vap. Dep.*, 1975, p. 270.

[7] J. B. MacChesney, P. B. O'Connor, F. V. DiMarcello, J. R. Simpson, and P. D. Lazay, "Preparational low loss optical fibers using simultaneous vapor phase deposition and fusion," in *Proc. 10th Int. Congr. Glass*, 1974, pp. 6-40–6-44.

[8] J. B. MacChesney, P. B. O'Connor, and H. M. Presby, "A new technique for preparation of low-loss and graded index optical fibers," *Proc. IEEE*, vol. 62, pp. 1278–1279, Sept. 1974.

[9] *Handbook of Chemistry and Physics*, vol. 49, 1969, pp. D112–116.

[10] R. L. Barns, E. A. Chandross, and C. M. Melliar-Smith, "The photochemical purification of reagents used in the MCVD process," in *Proc. 6th European Conf. Opt. Commun.*, York, England, 1980, pp. 26–28.

[11] K. Nassau, "The diffusion of water in optical fibers," *Mat. Res. Bull.*, vol. 13, pp. 67–76, 1978.

[12] B. J. Ainslie, P. W. France, and G. R. Newns, "Water impurity in low-loss silica fibre," *Mat. Res. Bull.*, vol. 12, pp. 481–488, 1977.

[13] H. Osanai, "Fabrication of ultra-low-loss, low-OH-content high silica optical fiber," in *Extended Abstr., Fall Meet. Electrochem. Soc.*, Pittsburgh, PA, 1978, pp. 367–369.

[14] M. Kawachi, M. Horiguchi, A. Kawana, and T. Mayashita, "OH-ion distribution in rod preforms of high-silica optical waveguides," *Electron. Lett.*, vol. 13, pp. 247–248, 1977.

[15] D. Gloge, "Propagation effects in optical fibers," *IEEE Trans. Microwave Theory Techn.*, vol. MTT-23, pp. 106–120, Jan. 1975.

[16] P. W. Black, J. Irven, K. Byron, I. S. Few, and R. Worthington, "Measurements on waveguide properties of GeO_2-SiO_2 cored optical fibers," *Electron. Lett.*, vol. 10, pp. 239–240, 1974.

[17] L. G. VanUitert, D. A. Pinnow, J. C. Williams, T. C. Rich, R. A. Jaeger, and W. H. Grodkiewicz, "Borosilicate glasses for fiber optical waveguides," *Mat. Res. Bull.*, vol. 8, pp. 469–476, 1973.

[18] D. N. Payne and W. A. Gambling, "A new silica-based low-loss optical fiber," *Electron. Lett.*, vol. 10, pp. 289–290, 1974.

[19] R. G. Sommer, R. D. DeLuca, and G. E. Burke, "New glass system for low-loss optical waveguides," *Electron. Lett.*, vol. 12, no. 16, pp. 408–409, 1976.

[20] A. Muhlick, K. Rau, F. Simmat, and N. Treber, "A new doped synthetic silica as a bulk material for low loss optical fibers," presented at the 1st European Conf. Opt. Fiber Commun., London, England, 1975.

[21] K. Abe, "Fluorine doped silica for optical waveguides," in *Proc. 2nd European Conf. Opt. Fiber Commun.*, Paris, France, 1976, pp. 59–61.

[22] H. Murata and N. Inagaki, "Low loss single-mode fiber development and splicing research in Japan," *IEEE J. Quantum Electron.*, vol. QE-17, pp. 835–849, June 1981.

[23] B. J. Ainslie, K. J. Beales, C. R. Day, and J. D. Rush, "Interplay of design parameters and fabrication conditions on the performance of monomode fibers made by MCVD," *IEEE J. Quantum Electron.*, vol. QE-17, pp. 854–857, June 1981.

[24] P. D. Lazay, A. D. Pearson, W. A. Reed, and P. J. Lemaire, "An improved single mode fiber design, exhibiting low loss, high bandwidth, and tight mode confinement simultaneously," Post-Deadline Paper, CLEO, Washington, DC, June 1981; L. G. Cohen and W. L. Mammel, "Tailoring the shapes of dispersion spectra to control bandwidths in single-mode fibers," presented at the 7th European Conf. Opt. Fiber Commun., Copenhagen, Denmark, 1981, paper 3.3.

[25] J. Irven, K. C. Byron, and G. J. Cannell, "Dispersion characteristics of practical single mode fibers," presented at the 7th European Conf. Opt. Fiber Commun., Copenhagen, Denmark, 1981, paper 4.3-1.

[26] D. Marcuse, D. Gloge, and E.A.J. Marcatili, "Guiding properties of fibers," in *Optical Fiber Telecommunications*, S. E. Miller and A. G. Chynoweth, Eds., 1979, pp. 37–100.

[27] P. C. Schultz, "Ultraviolet absorption of titanium and germanium in fused silica," in *Proc. 11th Int. Congr. Glass*, Prague, Czechoslovakia, vol. 3, pp. 155–163, 1977.

[28] V. Miya, Y. Terunuma, T. Hosaka, and T. Miyashita, "Ultra low loss single-mode fibers at 1.55 μm," *Electron. Lett.*, vol. 15, pp. 106–181, 1979.

[29] H. Osanai, T. Shioda, T. Moriyama, S. Araki, M. Horiguchi, T. Izawa, and H. Takata, "Effect of dopants on transmission loss of low-OH content optical fibres," *Electron. Lett.*, vol. 12, no. 21, pp. 549–550, 1976.

[30] T. Izawa, N. Shibata, and A. Takeda, "Optical attenuation in pure and doped fused silica in the IR wavelength region," *Appl. Phys. Lett.*, vol. 31, no. 1, pp. 33–35, 1979.

[31] J. Irven, "Long wavelength performance of $SiO_2/Geo_2/P_2O_5$ core fibers with different P_2O_5 levels," *Electron. Lett.*, vol. 17, no. 1, pp. 2–3, 1981.

[32] R. Olshansky, "Optical properties of waveguide materials for 1.2 to 1.8 μm," in *Physics of Fiber Optics, Advances in Ceramics*, vol. 2, B. Bendow and S. Mitra, Eds. 1981, pp. 40–46.

[33] K. Yoshida, Y. Furui, S. Sensui, and T. Kuroha, "Low-loss fibre under high deposition rate by MCVD technique," *Electron. Lett.*, vol. 13, no. 20, pp. 608–610, 1977.

[34] W. A. Gambling, D. N. Payne, C. R. Hammond, and S. R. Norman, "Optical fibers based on phosphosilicate glass," *Proc. IEE*, vol. 123, no. 6, pp. 570–575, June 1976.

[35] J. Schroeder, R. Mohr, P. B. Macedo, and C. J. Montrose, "Rayleigh and Brillouin scattering in K_2O-SiO_2 glasses," *J. Amer. Ceram. Soc.*, vol. 56, no. 10, pp. 510–514, 1973.

[36] M. Horiguchi and H. Osanai, "Spectral losses of low-OH content optical fibers," *Electron. Lett.*, vol. 12, no. 12, pp. 310–312, 1976.

[37] M. G. Blankenship, D. B. Keck, P. S. Leven, W. F. Love, A. Sarkar, P. C. Schultz, K. D. Sheth, and R. W. Siegfried, Post Deadline Papers, Conf. Opt. Fiber Commun., Washington, DC, 1979.

[38] C. R. Kurkjian and G. E. Peterson, "Some material problems in the design of glass fiber optical waveguides," in *Proc. 2nd Cairo Solid State Conf.*, vol. 2, 1973, p. 61.

[39] P. C. Schultz, "Optical absorption of the transition elements in vitreous silica," *J. Amer. Ceram. Soc.*, vol. 57, no. 7, pp. 309–313, 1974.

[40] P. Kaiser, "Spectral losses of unclad fibers made from high grade vitreous silica," *Appl. Phys. Lett.*, vol. 23, no. 1, pp. 45–46, 1973.

[41] D. B. Keck, R. D. Maurer, and P. C. Schultz, "On the ultimate lower limit of attenuation in glass optical waveguides," *Appl. Phys. Lett.*, vol. 22, no. 7, pp. 307–309, 1973.

[42] N. Shibata, M. Kawachi, and T. Edahiro, "Optical loss characteristics of high GeO_2 content silica fibers," *Trans. IECE Japan*, vol. 63, no. 12, pp. 837–841, 1980.

[43] Y. Mita, S. Matsushita, T. Yanase, and H. Nomura, "Optical absorption characteristics of hydroxyl radicals in phosphorous-containing silica glass," *Electron. Lett.*, vol. 13, no. 2, pp. 55–56, 1977.

[44] T. Edahiro, M. Horiguchi, K. Chida, and Y. Ohmori, "Spectral loss characteristics of GeO_2-P_2O_5 doped silica graded index fibres in long-wavelength band," *Electron. Lett.*, vol. 15, no. 10, pp. 274–275, 1979.

[45] K. Inada, "A new graphical method relating to optical fiber attenuation," *Opt. Commun.*, vol. 19, no. 3, pp. 437–439, 1976.

[46] P. Kaiser, "Drawing induced coloration in vitreous silica fibers," *J. Opt. Soc. Amer.*, vol. 64, pp. 475–481, 1974.

[47] R. Yamauchi, T. Kobayashi, T. Arai, and K. Inada, "Coloration and its reduction in phosphorous-doped low-loss fibres," *Electron. Lett.*, vol. 13, no. 16, pp. 461–462, 1977.

[48] K. Yoshida, "Optical fiber drawing and its influence on fiber loss," in *Tech. Dig. IOOC*, Japan, 1977, pp. 327–330.

[49] L. L. Blyler, Jr., F. V. DiMarcello, J. R. Simpson, E. A. Sigety, A. C. Hart, Jr., and V. A. Foertmeyer, "UV-radiation induced losses in optical fibers and their control," *J. Non-Cryst. Solids*, vol. 38, pp. 165–170, 1980.

[50] F. T. Stone and B. R. Eichenbaum, "Added optical loss in graded-index germanium-phosphosilicate-core fibers caused by UV radiation," *J. Non-Cryst. Solids*, vol. 38, pp. 189–194, 1980.

[51] E. J. Friebele, "Optical fiber waveguides in radiation environ-

ments," *Opt. Eng.*, vol. 18, no. 6, pp. 552-561, 1979.
[52] D. Gloge and E.A.J. Marcatili, "Multimode theory of graded-core fibers," *Bell Syst. Tech. J.*, vol. 52, pp. 1563-1578, 1973.
[53] R. Olshansky and D. B. Keck, "Pulse broadening in graded-index optical fibers," *Appl. Opt.*, vol. 15, no. 2, pp. 483-491, 1973.
[54] S. E. Miller, E. A. Marcatili, and T. Li, "Research toward optical fiber transmission systems–Part II: Devices and systems considerations," *Proc. IEEE*, vol. 61, pp. 1726-1751, Dec. 1973.
[55] D. N. Payne and W. A. Gambling, "Zero material dispersion in optical fibres," *Electron. Lett.*, vol. 11, no. 8, pp. 176-178, 1975.
[56] I. H. Mallitson, "Interspecimen comparison of the refractive index of pure fused silica," *J. Opt. Soc. Amer.*, vol. 55, pp. 1205-1209, 1965.
[57] F.M.E. Sladen, D. N. Payne, and M. J. Adams, "Measurement of profile dispersion in optical fibres: A direct technique," *Electron. Lett.*, vol. 13, pp. 212-213, 1977.
[58] S. Kobayashi, S. Shibata, N. Shibata, and T. Igawa, "Refractive index dispersion of doped fused silica," in *Proc. Int. Conf. Int. Opt. and Opt. Fiber Commun.*, Tokyo, Japan, 1977, pp. 309-312.
[59] D. N. Payne and A. H. Hartog, "Determination of the wavelength of zero material dispersion in optical fibres by pulse-delay measurements," *Electron. Lett.*, vol. 13, pp. 627-629, 1977.
[60] J. W. Fleming, "Material and mode dispersion in GeO_2-B_2O_3-SiO_2 glasses," *J. Amer. Ceram. Soc.*, vol. 59, no. 11-12, pp. 503-507, 1976.
[61] C. Lin, L. G. Cohen, W. G. French, and V. A. Foertmeyer, "Pulse delay measurements in the zero material dispersion region for germanium and phosphorous-doped silica fibres," *Electron. Lett.*, vol. 14, pp. 170-172, 1978.
[62] L. G. Cohen and C. Lin, "Pulse delay measurements in zero material dispersion wavelength region for optical fibers," *Appl. Opt.*, vol. 16, no. 12, pp. 3136-3139, 1977.
[63] J. W. Fleming, "Material dispersion in lightguide glasses," *Electron. Lett.*, vol. 14, no. 11, pp. 326-328, 1978.
[64] I. P. Kaminow and H. M. Presby, "Binary silica optical fibers: Refractive index and profile dispersion measurements," *Appl. Opt.*, vol. 15, no. 12, pp. 3029-3036, 1976.
[65] Y. Ohmori, K. Chida, M. Horiguchi, and I. Hatakeyama, "Optimal profile parameter on graded index optical fibre at 1.27 μm wavelength," *Electron. Lett.*, vol. 14, no. 24, pp. 764-765, 1978.
[66] E.A.J. Marcatili, "Modal dispersion in fibers with arbitrary numerical aperture and profile dispersion," *Bell Syst. Tech. J.*, vol. 56, pp. 49-63, 1977.
[67] G. E. Peterson, A. Carnevale, D. W. Berreman, and U. C. Paek, "A rigorous solution to Maxwell's equations for lightguides," *J. Non-Cryst. Solids*, vol. 38, pp. 221-226, 1980.
[68] D. Marcuse and H. M. Presby, "Calculation of bandwidth from refractive index profiles," *Appl. Opt.*, vol. 18, no. 22, pp. 3758-3763, 1979.
[69] M. Horiguchi, Y. Ohmori, and H. Takata, "Profile dispersion characteristics of high bandwidth graded-index fibers," *Appl. Opt.*, vol. 19, no. 18, pp. 3159-3167, 1980.
[70] D. Gloge, "Dispersion in weakly guiding fibers," *Appl. Opt.*, vol. 10, no. 11, pp. 2442-2445, 1971.
[71] A. Sugimura, K. Daikoku, N. Omoto, and T. Miya, *IEEE J. Quantum Electron.*, vol. QE-16, pp. 215-225, Feb. 1980.
[72] R. Olshansky, "Distortion losses in cabled optical fibers," *Appl. Opt.*, vol. 14, no. 1, pp. 20-21, 1975.
[73] C. M. Miller and S. C. Mettler, "A loss model for parabolic-profile fiber splices," *Bell Syst. Tech. J.*, vol. 57, no. 9, pp. 3167-3180, 1978.
[74] S. Seikai, N. Kashima, K. Kitayama, and N. Uchida, "Optimum design of graded index fiber structure," in *Tech. Dig. 3rd IOOC*, Washington, DC, 1979, pp. 100-102.
[75] W. B. Gardner, S. R. Nagel, M. I. Schwartz, F. V. DiMarcello, C. R. Lovelace, D. L. Brownlow, M. R. Santana, and E. A. Sigety, "The effect of fiber core and cladding diameter on the loss added by packaging and thermal cycling," *Bell Syst. Tech. J.*, vol. 60, no. 6, pp. 859-864, 1981.
[76] F. V. DiMarcello, A. C. Hart, Jr., J. C. Williams, and C. R. Kurkjian, "High strength funace-drawn optical fibers," in *Fiber Optics: Advances in Research and Development*, B. Bendow and S. S. Mitra, Eds. New York: Plenum, 1979, pp. 125-135.
[77] D. L. Powers, "Kinetics of $SiCl_4$ oxidation," *J. Amer. Ceram. Soc.*, vol. 61, no. 7-8, pp. 295-297, 1978.
[78] W. G. French, L. J. Pace, and V. A. Foertmeyer, "Chemical kinetics of the reactions of $SiCl_4$, $SiBr_4$, $GeCl_4$, $POCl_3$, and BCl_3 with oxygen," *J. Phys. Chem.*, vol. 82, pp. 2191-2194, 1978.
[79] D. L. Wood, J. B. MacChesney, and J. P. Luongo, "Invesitgation of the reactions of $SiCl_4$ and O_2 at elevated temperatures by infrared spectroscopy," *J. Mat. Sci.*, vol. 13, pp. 1761-1768, 1978.
[80] P. Kleinert, D. Schmidt, J. Kirchhof, and A. Funke, "About oxidation of $SiCl_4$ and $GeCl_4$ in homogeneous gas phase," *Kristall und Technik*, vol. 15, no. 9, pp. 85-90, 1980.
[81] D. L. Wood, K. L. Walker, J. R. Simpson, J. B. MacChesney, D. L. Nash, and P. Angueira, "Chemistry of the MCVD process for making optical fibers," in *Proc. 7th ECOC*, Copenhagen, Denmark, 1981, pp. 1.2-1-1.2-4.
[82] D. L. Wood *et al.*, private communication.
[83] K. L. Walker, J. B. MacChesney, and J. R. Simpson, "Reduction of hydroxyl contamination in optical fiber preforms," in *Tech. Dig. 3rd Int. Conf. Int. Opt. and Opt. Fiber Commun.*, San Francisco, CA, 1981, pp. 86-88.
[84] D. L. Wood, T. Y. Kometani, J. P. Luongo, and M. A. Saifi, "Incorporation of OH in glass in the MCVD process," *J. Amer. Ceram. Soc.*, vol. 62, no. 11-12, pp. 638-639, 1979.
[85] D. L. Wood and J. S. Shirk, "Partition of hydrogen in the modified chemical vapor deposition process," *J. Amer. Ceram. Soc.*, vol. 64, no. 6, pp. 325-327, 1981.
[86] C. LeSergent, M. Liegois, and Y. Floury, "Influence of the purity of reagents on the attenuation of CVD made doped silica optical fibers," *J. Non-Cryst. Solids*, vol. 38-39, pp. 263-268, 1980.
[87] A. D. Pearson, "Hydroxyl contamination of optical fibers and its control in the MCVD process," in *Tech. Dig. 6th European Conf. Opt. Fiber Commun.*, York, England, 1980, pp. 22-25.
[88] B. J. Ainslie, C. R. Day, J. Rush, and K. J. Boules, "Optimized structure for producing long ultra-low loss single mode fibres," *Electron. Lett.*, vol. 16, no. 18, p. 692, 1980.
[89] P. G. Simpkins, S. Greenberg-Kosinski, and J. B. MacChesney, "Thermophoresis: The mass transfer mechanism in modified chemical vapor deposition," *J. Appl. Phys.*, vol. 50, no. 9, pp. 5676-5681, 1979.
[90] K. L. Walker, G. M. Homsy, and F. T. Geyling, "Thermophoretic deposition of small particles in laminar tube flow," *J. Colloid Interface Sci.*, vol. 69, no. 1, pp. 138-147, 1979.
[91] S. R. Nagel, K. L. Walker, and F. T. Geyling, "Thermophoretic deposition of small particles in the modified chemical vapor dispersion (MCVD) process," in *Tech. Dig. Opt. Fiber Commun.*, Washington, DC, 1979, paper WC2.
[92] K. L. Walker, F. T. Geyling, and S. R. Nagel, "Thermophoretic deposition of small particles in the modified chemical vapor deposition (MCVD) process," *J. Amer. Ceram. Soc.*, vol. 63, no. 9-10, pp. 552-558, 1980.
[93] K. L. Walker, J. W. Harvey, F. T. Geyling, and S. R. Nagel, "Consolidation of particulate layers in the fabrication of optical fiber preforms," *J. Amer. Ceram. Soc.*, vol. 63, no. 1-2, pp. pp. 96-102, 1980.
[94] S. Greenberg-Kosinski, L. Soto, S. R. Nagel, and T. Watrous, "Characterization of germanium phosphosilicate films prepared by modified chemical vapor deposition," presented at the Glass Division Meet., Amer. Ceram. Soc., Oct. 1981.
[95] D. Marcuse, "Calculation of bandwidth from index profiles of optical fibers, I. Theory," *Appl. Opt.*, vol. 18, no. 12, pp. 2073-2080, 1979.
[96] J. A. Lewis, "The collapse of a viscous tube," *J. Fluid Mech.*, vol. 81, no. 1, pp. 129-135, 1977.
[97] J. Kirchoff, "A hydrodynamic theory of the collapsing process for the preparation of optical waveguide preforms," *Phys. Status Solidi*, vol. 60, pp. 127-131, 1980.
[98] F. T. Geyling and K. L. Walker, "The collapse of optical fiber preform tubes," submitted to *J. Appl. Mech.*
[99] S. R. Nagel, S. G. Kosinski, K. L. Walker, and D. L. Brownlow, "Reduced cycle time MCVD," in *Tech. Dig. 3rd IOOC*, San Francisco, CA, 1981, paper WA6.
[100] W. G. French and G. W. Tasker, U.S. Patent 4 154 591.
[101] T. Akamatsu, K. Okamura, and Y. Ueda, "Fabrication of graded-index fibers without an index dip by chemical vapor deposition method," *Appl. Phys. Lett.*, vol. 31, no. 8, pp. 515-517, 1977.
[102] S. Hopland, "Removal of the refractive index dip by an etching method," *Electron. Lett.*, vol. 14, no. 24, pp. 757-759, 1978.
[103] L. L. Blyler, Jr. and F. V. DiMarcello, "Fiber drawing, coating, and jacketing," *Proc. IEEE*, vol. 68, pp. 1194-1198, Oct. 1980.

[104] F. V. DiMarcello, D. L. Brownlow, and D. S. Shenk, "Strength characterization of multikilometer silica fibers," in *Tech. Dig. 3rd IOOC*, San Francisco, CA, 1981, paper MG6.
[105] D. H. Smithgall and R. E. Frazee, "Automatic detection and centering of fibers in coatings," in *Tech. Dig. 3rd IOOC*, San Francisco, CA, 1981, paper TuG5.
[106] U. C. Paek and C. M. Schroeder, "High-speed coating of optical fibers at a rate greater than 5 m/sec," in *Tech. Dig. 3rd IOOC*, San Francisco, CA, 1981, paper WG2.
[107] R. B. Runk, "Processing control of optical fiber manufacture," in *Extended Abstr., Fall Meet. Electrochem. Soc.*, Pittsburgh, PA, 1978, pp. 365-366.
[108] M. Okada, M. Kawachi, and A. Kawana, "Improved chemical vapor deposition method for long-length optical fibre," *Electron. Lett.*, vol. 14, pp. 89-90, 1978.
[109] P. D. Lazay and W. G. French, "Control of substrate tube diameter during MCVD preform preparation," in *Tech. Dig. Opt. Fiber Commun.*, Washington, DC, 1979, paper WC3.
[110] R. B. Runk, "A zirconia induction furnace for drawing precision silica waveguides," in *Tech. Dig. Topical Meet. Opt. Fiber Transmission II*, Williamsburg, VA, 1977, paper TuB5.
[111] A. C. Hart, Jr. and R. V. Albarino, "An improved fabrication technique for applying coatings to optical fiber waveguides," in *Tech. Dig. Topical Meet. Opt. Fiber Transmission II*, Willamsburg, VA, 1977, paper TuB2.
[112] D. H. Smithgall, "On the control of the fiber drawing process," in *Tech. Dig. Opt. Fiber Commun.*, Washington, DC, 1979, paper WF4.
[113] R. J. Klaiber and M. I. Cohen, "Drawing of smooth optical fibers," in *Tech. Dig. Topical Meet. Opt. Fiber Transmission II*, Williamsburg, VA, 1977, paper TuB4.
[114] J. B. MacChesney, R. E. Jaeger, D. A. Pinnow, F. W. Ostermayer, T. C. Rich, and L. G. VanUitert, "Low-loss silica core-borosilicate clad optical waveguides," *Appl. Phys. Lett.*, vol. 23, no. 6, pp. 340-341, 1973.
[115] W. G. French, A. D. Pearson, G. W. Tasker, and J. B. MacChesney, "Low-loss fused silica optical waveguide with borosilicate cladding," *Appl. Phys. Lett.*, vol. 23, no. 6, pp. 338-340, 1973.
[116] T. Akamatsu, K. Okamura, and Y. Ueda, "Fabrication of long fibers by an improved chemical vapor deposition method (HCVD method)," *Appl. Phys. Lett.*, vol. 31, no. 3, pp. 174-176, 1977.
[117] P. B. O'Connor, J. B. MacChesney, and C. M. Melliar-Smith, "Large core high NA fibres for data link applications," *Electron. Lett.*, vol. 13, no. 7, pp. 170-171, 1977.
[118] K. Hoshida, Y. Furui, S. Sentsui, and T. Kuroha, "Low-loss fibre prepared under high deposition rate by modified CVD technique," *Electron. Lett.*, vol. 13, no. 20, pp. 608-609, 1977.
[119] S. R. Nagel and M. A. Saifi, "Effect of deposition rate on spectral loss of GeO_2-P_2O_5-SiO_2 graded index fibres," *Electron. Lett.*, vol. 16, no. 12, pp. 469-470, 1980.
[120] J. R. Simpson, J. B. MacChesney, K. L. Walker, and D. L. Wood, "MCVD preform fabrication at high deposition rates," *Phys. Fiber Opt., Advances in Ceramics*, vol. II, B. Bendow and S. S. Mitra, Eds., 1981, pp. 8-13.
[121] J. R. Simpson, J. B. MacChesney, and K. L. Walker, "High rate MCVD," *J. Non-Cryst. Solids*, vol. 38, pp. 831-836, 1980.
[122] M. Tsukamoto, K. Okamura, J. Goto, O. Nakamura, and T. Akamatsu, "Fabrication a large preform for a 40-km length of fiber using the CVD method," in *Tech. Dig. IOOC*, San Francisco, CA, 1981, paper WA2.
[123] A. D. Pearson, "Fabrication of single mode fiber at high rate in very long lengths for submarine cable," in *Tech. Dig. IOOC*, San Francisco, CA, 1981, paper WA2.
[124] M. I. Cohen, "Progress in multimode and single mode lightguides prepared by the MCVD process," in *Tech. Dig. Conf. Lasers and Electro-Opt.*, Washington, DC, 1981, paper WC1.
[125] R. E. Jaeger, J. B. MacChesney, and T. J. Miller, U.S. Patent 4 262 035; J. W. Fleming, J. B. MacChesney, and P. B. O'Connor, U.S. Patent pending.
[126] P. Geittner, D. Küppers, and H. Lydtin, "Low-loss optical fibers prepared by plasma-activated chemical vapor deposition (CVD)," *Appl. Phys. Lett.*, vol. 28, no. 11, pp. 645-646, 1976.
[127] J. W. Versluis and J.G.J. Peelen, "Optical communication fibres manufacture and properties," *Phlips Telecommun. Rev.*, vol. 37, no. 4, pp. 215-230, 1976.
[128] J. Irven and A. Robinson, "Optical fibers prepared by plasma augmented vapour deposition," *Phys. Chem. Glasses*, vol. 21, no. 1, pp. 47-52, 1980.
[129] R. E. Jaeger, J. B. MacChesney, and T. J. Miller, "The preparation of optical waveguide preforms by plasma deposition," *Bell Syst. Tech. J.*, vol. 57, no. 1, pp. 205-210, 1978.
[130] K. Fujiwara, N. Yoshioka, and M. Hoshika, "Optical fiber fabrication by isothermal plasma activated deposition," in *Proc. 3rd European Conf. Opt. Fiber Trans.*, Munich, Germany, 1977, pp. 15-17.
[131] J. W. Fleming and P. B. O'Connor, "High rate lightguide fabrication technique," *Phys. Fiber Opt. Adv. in Ceram.*, vol. II, B. Bendow and S. S. Mitra, Eds., 1981, pp. 21-26.
[132] J. W. Fleming, "Progress in plasma prep. of lightguides," presented at the 12th Int. Congr. Glass, Albuquerque, NM, Poster Session, 1980.
[133] J. W. Fleming and V. R. Raju, "Low optical attenuation fibers prepared by plasma enhanced MCVD," in *Tech. Dig. IOOC*, San Francisco, CA, 1981, paper WD2.
[134] ——, "Low loss single mode fibers prepared by plasma enhanced MCVD," submitted to *Electron. Lett.*
[135] S. R. Nagel and S. G. Kosinski, unpublished data.
[136] C. Lin, P. L. Liu, T. P. Lee, C. A. Burrus, F. T. Stone, and A. J. Ritger, "Measuring high bandwidth fibres in the 1.3 μm region with picosecond InGa injection lasers and ultrafast InGaAs detectors," *Electron. Lett.*, vol. 17, no. 13, pp. 438-440, 1981.
[137] F. Partus, Western Electric-PECC, reported by Cohen [124].
[138] Data Courtesy of Western Electric–Atlanta Works.
[139] P. C. Schultz, "Fabrication of optical waveguides by the outside vapor deposition process," *Proc. IEEE*, vol. 68, pp. 1187-1190, Oct. 1980.
[140] A. Sarkar, "Materials and processes of fiber fabrication," presented at the IEEE Commun. Workshop, Potsdam, NY, 1981.
[141] T. Izawa and N. Inagaki, "Materials and processes for fiber preform fabrication–vapor phase axial deposition," *Proc. IEEE*, vol. 68, pp. 1184-1187, Oct. 1980.
[142] F. Hanawa, S. Sudo, M. Kawachi, M. Nakahara, "Fabrication of completely OH-free VAD fibre," *Electron. Lett.*, vol. 16, no. 18, pp. 699-670, 1980.
[143] M. Nakahara, S. Sudo, N. Inagaki, K. Yoshida, S. Shibuya, K. Kukura, and T. Kuroha, "Ultra wide bandwidth VAD fibre," *Electron. Lett.*, vol. 16, no. 10, pp. 391-392, 1980.
[144] M. Nakahara, N. Inagaki, K. Yoshida, M. Yoshida, and O. Fukada, "Fabrication of 100-km graded-index fiber from a continuously consolidated VAD preform," in *Proc. IOOC*, San Francisco, CA, 1981, p. 100.

Suzanne R. Nagel was born in Jersey City, NJ, on October 4, 1945. She received the B.S. degree in ceramic engineering from Rutgers University, New Brunswick, NJ, in 1968, the A.B. degree in liberal arts from Douglas College in 1968, and the M.S. and Ph.D. degrees in ceramic engineering from the University of Illinois, Urbana, in 1970 and 1973, respectively.

In 1972 she joined Bell Laboratories as a member of the Technical Staff where she has been involved in research on materials and methods for fabricating lightguides for telecommunications. She is currently a Supervisor of the fiber materials and process technology group in the Crystal Growth R&D Department, Murray Hill, NJ.

Dr. Nagel is a member of the American Ceramic Society, the Optical Society of America, the National Institute of Ceramic Engineers, and the Society of Women Engineers.

J. B. MacChesney, photograph and biography not available at the time of publication.

Kenneth L. Walker was born in Denver, CO, on November 2, 1951. He received the B.S. in chemical engineering from the California Institute of Technology, Pasadena, in 1974, and the Ph.D. from Stanford University, Stanford, CA, in 1980.

In 1979, he joined Bell Laboratories, Murray Hill, NJ, as a member of the Technical Staff where he has been active in research on the physical phenomena involved in the fabrication of optical fibers.